

Thesis Formulation Report:  
Modelling of ice Crystal icing

Timothy F. Peters



at the  
Department of Mathematics,  
University of Bath,

Supervisors: Dr. Philippe Trinh  
Dr. Hui Tang

September 2021



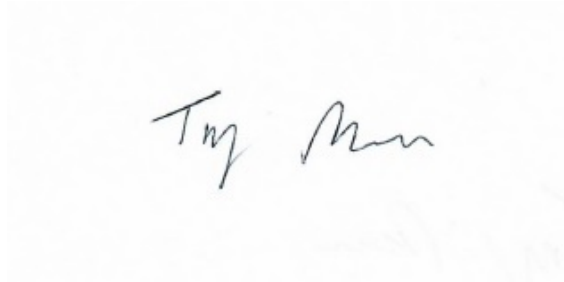
# Contents

<b>Declaration of Authorship</b>	<b>v</b>
<b>Abstract</b>	<b>vi</b>
<b>Responsible Research &amp; Innovation</b>	<b>vi</b>
<b>List of Abbreviations</b>	<b>vii</b>
<b>List of Mathematical Symbols</b>	<b>viii</b>
<b>List of Figures</b>	<b>ix</b>
<b>1 Introduction</b>	<b>1</b>
1.1 Background and motivation . . . . .	1
1.2 Model Evolution . . . . .	3
1.2.1 Historical Ice Accretion models . . . . .	3
1.2.2 Stefan Problem . . . . .	3
1.3 Structure of the report . . . . .	5
<b>2 Literature Review</b>	<b>7</b>
2.1 Response to ICI . . . . .	7
2.2 Condition Classification . . . . .	8
2.3 Experiments . . . . .	9
2.3.1 Experimental Facilities . . . . .	9
2.3.2 Prior Experiments . . . . .	10
2.4 Icing models and codes . . . . .	11
<b>3 Three Layer Accretion Model</b>	<b>17</b>
3.1 Formulating the model . . . . .	17
3.2 Nondimensionalisation . . . . .	20
3.2.1 Initial evolution of the water layer . . . . .	20
3.2.2 Three Layer Model . . . . .	21
3.3 Bucknell Reduction . . . . .	22
<b>4 An extended look into the Three Layer Thermodynamic Model</b>	<b>25</b>
4.1 Asymptotic behaviour for small Peclet number . . . . .	25
4.1.1 Water Layer . . . . .	25
4.1.2 Three Layer model . . . . .	27
4.2 Numerical Methodology of three layer problem . . . . .	28

---

4.2.1	Finite Difference of 3 Layer model . . . . .	28
4.2.2	Simulations . . . . .	31
<b>5</b>	<b>Summary, conclusions and outlook</b>	<b>35</b>
5.1	Summary and conclusions . . . . .	35
5.2	Future Work . . . . .	36
5.2.1	Next Steps . . . . .	36
5.2.2	Long Term . . . . .	36
	<b>Bibliography</b>	<b>38</b>
	<b>Appendix A</b>	<b>43</b>

# Declaration of Authorship

A rectangular box containing a handwritten signature in black ink. The signature appears to read "Tom Munn".

Signed:

---

# Abstract

A theoretical exploration of ice crystal icing. Historical and current literature is reviewed and further work is studied on a one-dimensional model of ice accretion corresponding to mixed/glaciated conditions for a hot substrate. A three layer thermodynamic accretion model is developed on the basis of a multiphase Stefan problem and then reduced to the original concept of design from the literature. Asymptotic solutions are found for the pseudo steady state and numerical results are obtained (via MATLAB) which show the transition from the single water layer to the proposed three layer model as key parameters are adjusted.

## **Responsible Research & Innovation**

My research is based on the theory of ice crystal icing in engines which is in the fields of applied mathematics, mechanical engineering and physics. However, the work I am carrying out is from a purely theoretically point of view. Naturally the project needs to be carried out with rigour, transparency as well as being accessible in case it impact other fields. The research in question has no sensitive data and does not concern itself with data storage. Carrying it out holds no ethical or social controversies. In the best case scenario for our research, it shortens the time-frame by which this ice crystal icing is understood, leading to more sustainable engines and safer flights.

## List of Abbreviations

EASA – European Aviation Safety Agency  
EIWG – Engine Icing Working Group,  
EMM – Extended Messinger Model,  
EMM-C – Extended Messinger Model-Crystals,  
EMM-ICI – Extended Messinger Model-Ice Crystal Icing,  
HAIC – High Altitude Ice Crystal  
HIWC - High Ice Water Content  
ICC – Ice Crystal Consortium  
ICI – Ice crystal icing  
IWC – Ice Water Content,  
MM – Messinger Model,  
MMD – Mass Mean Diameter,  
MR – Melt Ratio,  
NASA - National Aeronautics and Space Administration  
NRCC – National Research Council Canada  
ONERA – Office Nationald’Etudes et de Recherches Aérospatiale,  
RAE – Royal Airforce Establishment,  
RATFac – Research Altitude Testing Facility,  
SLD – Supercooled Liquid Droplets  
SLW – Supercooled Liquid Water  
TLC – Total Liquid Content  
TWC – Total Water Content

## List of Mathematical Symbols

$A_i$  – shear stress,

$c_i$  – heat capacity of substance  $i$ ,

$C'$  – inverse capillary number,

$\mathcal{F}$  – heat source/sink,

$h_i$  – height of layer  $i$ ,

$k_i$  – thermal conductivity of substance  $i$ ,

$L$  – characteristic length scale,

$L_m$  – latent heat of melting,

$La$  – unspecified latent heat,

$\dot{m}$  – mass flux,

$p$  – pressure,

$Q_i$  – fluid flux,

$q_i/r_i$  – heat flux terms,

$s_i$  – direction of principal curvature,

$T_i$  – temperature of layer  $i$ ,

$t$  – time

## Greek symbols used

$\kappa$  – curvature,

$\rho_i$  – density of substance  $i$ ,

$\sigma$  – surface tension,

## Nondimensional symbols used

$B$  – Bond number  $\mathcal{M}$  – mass flux,

Pe – Peclet number,

$Q$  – heat term,



St – Stefan number,



# List of Figures

1.1	Locations of the 46 flights that were further studied [Mason et al., 2006]. . . . .	2
1.2	EASA icing envelope regulations before 2015 and post 2015. . . . .	2
1.3	Rough schematic of the Stefan problem evolution over time for a layer of water and ice on a surface $0 \leq x \leq a$ with a warm substrate at $x = 0$ . . . . .	4
2.1	Severity of icing versus the ratio LWC/TWC. Figure from Currie and Fuleki [2015]	8
2.2	Scatterplot of the equivalent diameter MDD for ice particles with TWC larger than $0.5 \text{ g/cm}^3$ for the 3 flights. Figure from [Leroy et al., 2015] . . . . .	9
2.3	Boxplot of the distribution of the size of particles for given thresholds of TWC. Figure from Leroy et al. [2015] . . . . .	9
2.4	The RATFac where ice accretion physics research has been performed Currie et al. [2011]. Figure from Currie et al. [2011]. . . . .	10
2.5	Accretion growth of a cylindrical test article as performed by Currie and Fuleki [2015] showing both the perspective and side view. Figure from Currie and Fuleki [2015]. . . . .	11
2.6	Experiment performed by Bucknell et al. [2019b] showing the ice accretion at different stages of the experiment. Different stages are (a) 33% of duration; (b) 66%; (c) end of test. The $\text{TWC} = 4 \text{ g/m}^3$ . Figure from Bucknell et al. [2019b]	12
2.7	Set of energy transfer modes considered by Tribus [1949]. Figure from Oliver [2013]	13
2.8	Flow chart of the MTM code. Figure from [Oliver, 2013]. . . . .	13
2.9	Overveiw of the IGLOO2D showing the four main components. Figure from [Trontin and Villedieu, 2018] . . . . .	14
2.10	Different processes in the revisited MM for ICI. Different mass fluxes correspond to impinging ice particles, deposited ice particles, runback water incoming, evaporation, erosion, outgoing runback water and accretion of ice and water trapped within the ice. Figure from [Trontin and Villedieu, 2018]. . . . .	14
3.1	Schematic for the three layer model depicting the different heights and interfaces.	19
4.1	These plots show the heights (left) and temperatures (right) as a function of time obtained through numerical simulations of the three-layer model. Figures on the left show the height profile for $t \in [0, \bar{t} + t^*]$ . Those on the right show the temperature profile at $\bar{t} + t^*$ . We use default values of $Pe_w = 1$ , $St_w = 1$ , $St_i = 1$ , $\mathcal{F} = 0.75$ for insets (a) and (b). Inset (c) and (d) uses the same values but with $\mathcal{F} = 0.9$ . Similarly insets (e) and (f) use $Pe = 0.25$ . . . . .	32

---

<p>4.2 These plots show the heights (left) and temperatures (right) as a function of time obtained through numerical simulations of the three-layer model. Figures on the left show the height profile for <math>t \in [0, \bar{t} + t^*]</math>. Those on the right show the temperature profile at <math>\bar{t} + t^*</math>. We use default values of <math>Pe_w = 1</math>, <math>St_w = 1</math>, <math>St_i = 1</math>, <math>\mathcal{F} = 0.75</math>. Inset (a) and (b) use <math>St_w = 0.75</math> while insets (c) and (d) use <math>St_i = 0.9</math>. . . . .</p>	<p>33</p>
----------------------------------------------------------------------------------------------------------------------------------------------------------------------------------------------------------------------------------------------------------------------------------------------------------------------------------------------------------------------------------------------------------------------------------------------------------------------------------------------------------------------------------------------------------------------------------	-----------

# Chapter 1

## Introduction

This TFR is motivated by a need to develop mathematical models for the analysis of ice-crystal formation for a hot engine core. In particular, we develop and extend from a recent three-layer model proposed by the Oxford Thermofluids group. We non-dimensionalise the model, isolating key non-dimensional quantities and use asymptotic analysis in the pseudo steady state regime. Finally, we implement a numerical scheme to study the full system as the key quantities are swept.

In this chapter, we present a motivation for this project, including some background of problems caused over the years. We then give a brief evolution of the model upon which most current research is done. Finally, we set out the structure of this report.

### 1.1 Background and motivation

The jet engine plays a significant role in the modern world, being widely used in powered flight. Used for transport, defense or commercial reasons, the jet engine is global and an essential cog of how the world functions. Looking at 2019, there was a record number of 68,948,849 flights with the size of the commercial aircraft market being worth \$79.9 billion. Due to COVID-19, predicted growth of both number of passengers and engines deviated from expectation, with the total number of tracked flights dropping 27% to just below 50,000,000 flights. However, this is something which is steadily on the rise again.

It is well understood that certain atmospheric conditions are quite unfavourable towards engines in flights. Volcanic ash, sand, water and ice along with other substances can cause problems which result in engine damage, and in the worst cases to engine failure. The “Ice Particle Threat to Engines in Flight” by [Mason et al. \[2006\]](#) challenged the prior beliefs concerning the danger of different water/ice particles found in atmosphere. These can be generalised to supercooled liquid water (SLW) and supercooled large droplets (SLD). At the time, the term “icing” was used in relation to the accretion of the SLW on the aircraft and this was well documented with the regulations for aircraft already being well defined. In addition, it was assumed that ice particles were favourable to the engine as the particles were thought to just bounce off and thus no accretion would take place. From exploring the effect that ice particles cause in engines this has led to a renewed interest to better account for such conditions and led to the new terminology of “ice crystal icing” for the case of SLD. The study showed that from 240 recorded icing events over a 15 year period, 62 of them were classified as turbofan powerloss most likely

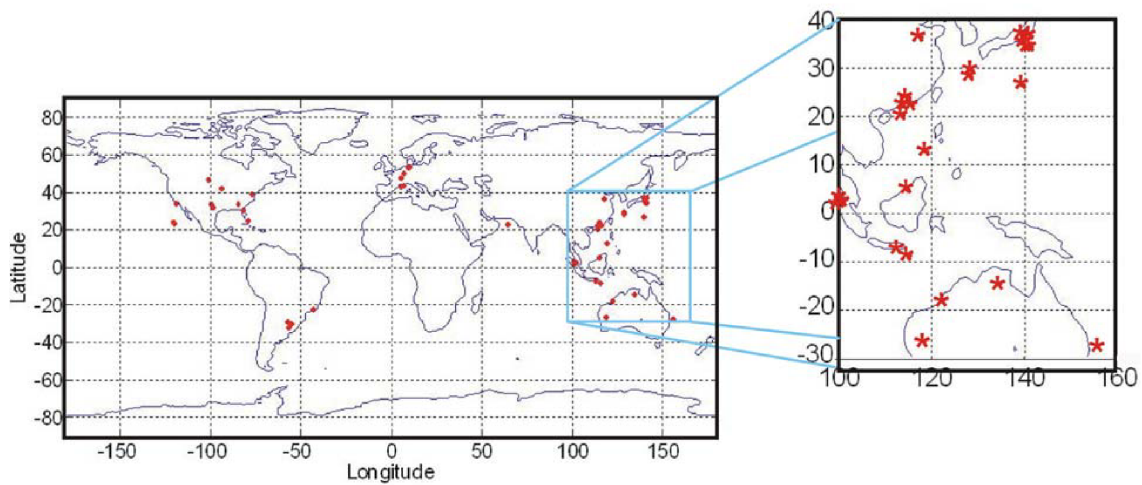


FIGURE 1.1: Locations of the 46 flights that were further studied [Mason et al., 2006].

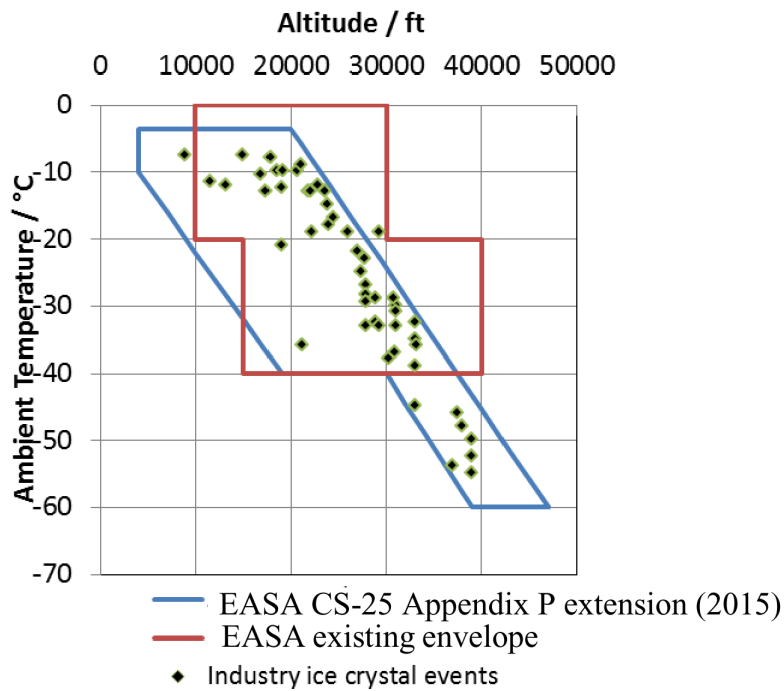


FIGURE 1.2: EASA icing envelope regulations before 2015 and post 2015.

as a result of these large ice particles. Of these, 46 were analysed further due to more complete data which can be seen in Figure 1.1

Having showed that a significant portion of these powerloss events occurred at altitudes outside the standard Federal Aviation Administration (FAA) engine certificate envelope, this led to the Engine Harmonization Working Group (EHWG) proposing that a new framework be designed such that both glaciated (only ice crystals) and mixed phase (ice crystals and supercooled water) conditions be accounted for. This new envelope is shown in Figure 1.2.

## 1.2 Model Evolution

### 1.2.1 Historical Ice Accretion models

Until the work of Tribus in 1949 [Messinger, 1952, 1953], very little study had been undertaken on an unheated icing surface. Prior to the point, much of the work had been done on heated surfaces and measures were taken to prevent it from occurring. The mindset was one of anti-icing rather than de-icing. Tribus established a model [Tribus, 1949] which would give an indication of how ice would grow. This would then allow for intermittent heating to then de-ice the surface. His model would give an indication of how much heat would be needed and how often. He considered two different regimes. He considered the two cases of when *SLW* impinged on either a surface equilibrium temperature which was below freezing, or above. In the first case, the liquid would freeze upon impact and thus ice would start to accrete, while in the latter, no ice accreted.

A few years later, Bernard Messinger [Messinger, 1953] recognised the absence of a third regime, that being when the equilibrium temperature corresponded with the freezing temperature. In this case, it results in a combined effect of the two other regimes where a portion of the water may freeze. He extended the Tribus model to allow for this third regime which led to the idea of a freezing fraction. This results in some fraction between 0 and 1 of the impinging water freezing on impact. Although presented in the 1950s this formed the basis for many of the ice prediction codes used today.

The Tribus and Messinger models are essentially an energy balance. This balance examines the heat lost from the incoming water and ice particles along with the energy gained from ice growth. By equating the heat gained from processes such as latent heat, heating and the incoming kinetic energy of droplets to the heat lost from evaporation, convective heat transfer and cooling, this provided an estimate for the freezing fraction. The type of ice growth expected would then depend on the freezing fraction obtained. For a value obtained between 0 and 1, this would indicate the growth of “glaze ice” – wet accretion – whereas a value above 1 would indicate “rime ice” – dry accretion.

Although this gave an indication of what fraction of ice would freeze, there were still important details missing such as the temperature profiles of the ice and water layers that could form. In the early 2000’s this was explored by Myers et al. [2002] who proposed the Extended Messinger Model (EMM) which examined the temperature profile of the difference layers. The interface between the water and ice is then described by the Stefan problem (which is discussed further in the next section). The heat balance from the above Messinger Model (MM) would still be incorporated into this new model, through a heat flux boundary condition on the top layer. As a result, all the Messinger energy terms appear in the EMM, however this new model accounts for the temperature profiles.

Since then there have been many adjustments of the MM and the EMM and these are foundational for much of the work carried out today.

### 1.2.2 Stefan Problem

The Stefan problem has long been used as a way of modelling phase change between two media. Originally motivated by Stefan in 1889 [Vuik, 1993] as a way of studying the formation of sea

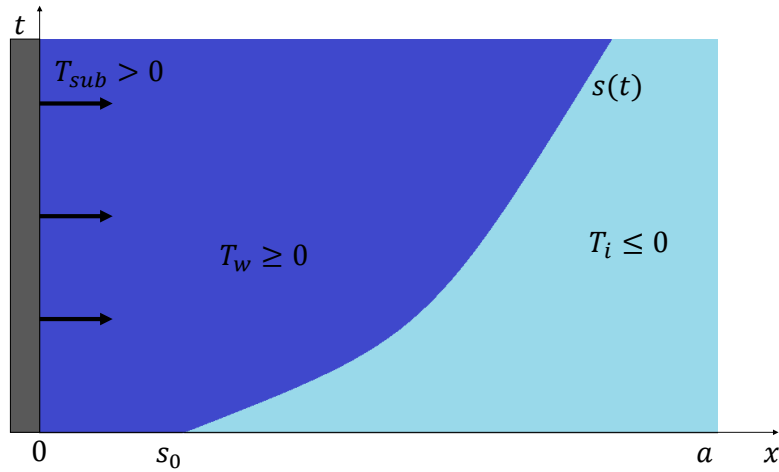


FIGURE 1.3: Rough schematic of the Stefan problem evolution over time for a layer of water and ice on a surface  $0 \leq x \leq a$  with a warm substrate at  $x = 0$ .

ice, the methodology lends itself quite naturally to studying the interaction between layers of water and ice.

The Stefan problem looks to understand how the interface between two media evolves over time and is therefore seen as a free or moving boundary problem. When a medium is heated/cooled the temperature increases/decreases as a result. However, when it comes to a change of phase, this results in the absorption or release of latent heat while keeping the temperature of the medium constant.

Mathematically, there exist PDEs describing the media above and below the interface which are not necessarily valid at the interface. The Stefan condition is needed to ensure a full system where this condition tracks the velocity of the moving boundary. The location of the moving boundary is driven by the temperature gradients on either side of the boundary. Suppose there is water and ice on  $x \in [0, a]$  such as in Figure 1.3. Here we have either a warm surface with above freezing temperature or an incoming heat flux on the left boundary and the initial interface as shown at  $s_0$ . Over time the incoming flux will heat the water, which results in a slow moving of the water-ice interface as the ice slowly melts. A typical two phase Stefan problem can be fully described by the following set of equations

$$\begin{aligned}
 & \left. \begin{aligned}
 c_1 \rho_1 \frac{\partial T_1}{\partial t} &= K_1 \frac{\partial^2 T_1}{\partial x^2}, & 0 < x < s(t) \\
 c_2 \rho_2 \frac{\partial T_2}{\partial t} &= K_2 \frac{\partial^2 T_2}{\partial x^2}, & s(t) < x < a
 \end{aligned} \right\} & \text{Heat Equations} \\
 & \left. \begin{aligned}
 L_f \rho_1 \frac{ds}{dt} &= K_2 \frac{\partial T_2}{\partial x} - K_1 \frac{\partial T_1}{\partial x} + Q(t), & x = s(t) \\
 T_1(s, t) &= T_2(s, t) = T_0
 \end{aligned} \right\} & \text{Stefan Conditions} \\
 & \left. \begin{aligned}
 s(0) &= s_0, & 0 < s_0 < a \\
 T_1(x, 0) &= T_{1,0}, & T_2(x, 0) = T_{2,0}
 \end{aligned} \right\} & \text{Initial Conditions} \\
 & \left. \begin{aligned}
 T_1(0, t) &= f_1(t), & \frac{\partial T_1}{\partial x} \Big|_{x=0} &= g_1(t) \\
 T_2(a, t) &= f_2(t), & \frac{\partial T_2}{\partial x} \Big|_{x=a} &= g_2(t)
 \end{aligned} \right\} & \text{Boundary Conditions}
 \end{aligned} \tag{1.1}$$



For  $i = 1, 2$ , we have that  $c_i$  is the heat capacity,  $\rho_i$  is the density,  $K_i$  is the thermal conductivity and  $T_i$  is the temperature of medium  $i$ . In addition  $F(t)$  represents any heat sources or sinks and  $L$  is the latent heat for the medium (e.g melting, vaporisation, etc).

For this to have any physical meaning, the initial data must be coherent. This means that  $T_1 \leq T_0 \leq T_2$  or  $T_2 \leq T_0 \leq T_1$ . For an ice water interface, the temperature is usually at melting temperature. A further simplification can be made in the Stefan condition if the ice layer is at a constant temperature in which case the gradient just becomes zero.

In the case where the moving boundary  $s(t)$  reaches either  $x = 0, a$  at some time  $t^*$ , this results in the disappearance of one of the media and the problem needs to be reformulated.

The two phase problem can be generalised quite easily to handle more layers. For each layer we need the two Stefan conditions along with sufficient boundary/initial conditions to specify a temperature profile. This idea is used later when we look to modify the work done by Bucknell.

**Note:** Mass and momentum also need to be conserved. If the density for the different media are the same (reasonable approximation for solid/liquid interface but not liquid/gas) then there is no relative motion. Otherwise, the difference in densities results in a velocity to account for the mass balance.

### 1.3 Structure of the report

The remainder of this report will be structured as follows.

In chapter 2 we undertake a literature review of the field. This encompasses our present understanding of the physical mechanisms which influence ice accretion, the different experimental groups and prior experiments, different numerical models and mechanisms which lead to engine damage.

In chapter 3 we explore the idea of the three layer model as proposed by the Oxford Thermofluids group starting with the full set of equations and subsequently breaking it down to the form as originally proposed by the Oxford Thermofluids group. We derive the full nondimensionalisation set of equations describing the system.

In chapter 4 we explore the full nondimensional system for the one dimensional case. We initially look at the asymptotics of the pseudo steady form. We then lay out the methodology for the numerics used to examine the full system with our results.

In Chapter 5 we summarise the work done over the course of this project, and provide a brief commentary on the possible future research based on the results obtained.



## Chapter 2

# Literature Review

Over the last 20 years, there has been an increasing number of collaborations between different countries and corporations in order to improve the state of the art knowledge regarding Ice Crystal Icing (ICI).

### 2.1 Response to ICI

With an increased understanding of the dangers posed by large ice crystals this led to world action, with different collaborative projects being formed to combat this new perceived threat. An immediate response to the problem presented by [Mason et al. \[2006\]](#) led to the Engine Icing Working Group being set up in 2007 with a further subgroup the Ice Crystal Consortium (ICC) also initiated to develop a roadmap moving forward. A few years later, both the High Altitude Ice Crystals (HAIC, Europe) and High Ice Water Content (HIWC, US) were formed with similar objectives. From a report of the HAIC [[Grandin and Dezitter, 2011](#)], these objectives can be summarised as follows:

- High altitude classification: Measuring different Ice Water Content (IWC), Liquid Water Content (LWC) and Mean Mass Diameters (MMD) for different altitude levels ,
- Measurement and detection of conditions: Development of equipment to both measure the glaciated/mixed ice content in test flights and also equipment to detect above conditions,
- Development of wind tunnels for experimentation: Tunnels which can simulate mixed/glaciated conditions,
- Development of ice accretion models: Developing a better understanding of the physics underlying ice accretion,
- Tracking of particles: Important to understand the particle trajectories as they move through the engine, how their shape is affected and identifying the key parameters ,
- Experiments to validate models: Perform tests in the glaciated/mixed conditions by which the models can be verified.

Although this work has been focused primarily on examining the developed accretion models, we shall motivate this by briefly discussing the other challenges presented by the HAIC report.

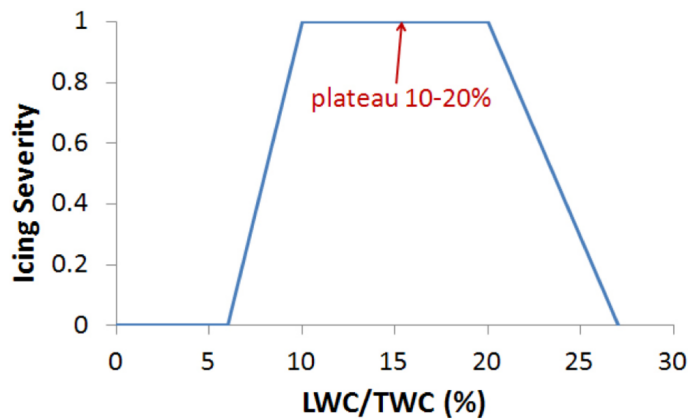


FIGURE 2.1: Severity of icing versus the ratio LWC/TWC. Figure from [Currie and Fuleki \[2015\]](#)

## 2.2 Condition Classification

With the new understanding of the damage able to be done to engines by ice particles, the natural progression was study under what conditions these ice crystals exist and are the most dangerous. From the study performed by [Mason et al. \[2006\]](#), it was postulated that the seriousness of the ice particles was related to the ratio between the Liquid Water Content (LWC) and the Total Water Content (TWC). This ended up being experimentally validated by [Currie and Fuleki \[2015\]](#). The basis for this theory was that for a glaciated environment, solid ice particles will just bounce off a surface whereas if there is too much water liquid content, the ice does not stick either. The relationship between the severity and this LWC/TWC ratio is shown as produced in Currie et al. in Figure 2.1.

**Note:** In other studies, this ratio between LWC and TWC in the icing cloud is referred to as the Melting Ratio (MR).

Knowing the impact that different LWC and Ice Water Content (IWC) had on glaciated conditions led to a joint effort between the HAIC and the HIWC in order to characterise regions of different IWC and to better understand the composition of said IWC. A field campaign was led in Darwin Australia in 2014 [[Leroy et al., 2015](#)]. Over the course of 23 flights, data concerning the composition, size and concentration were recorded and subsequently analysed. In Figures 2.2 and 2.3 we show results from three of the flights regarding the mass size of particles in relation to TWC. With regards to Figure 2.3 we can observe difference regimes for the different flights. While we see that flight 13 seems to have a large proportion of large particles and flight 16 has a much higher concentration of small particles, we see a combination of the two in flight 12.

From the field campaign in Darwin, a lot of useful data was collected regarding the size and concentration of ice particles in high IWC conditions. Having established that the accretion of ice particles needs a threshold LWC, the question of tracking particles as they enter the engine became a concern since for glaciated conditions, the liquid content needed for ICI often comes about via the melting of ingested particles. This has led to the further development of the different prerequisites needed for an accurate accretion model. Firstly, tracking of the particle is performed as it makes its way through the engine [[Gent et al., 2000](#), [Ayan and Özgen, 2018](#), [Bucknell et al., 2019c](#)]. After that, studying how a nonspherical particle evolves as it is melting

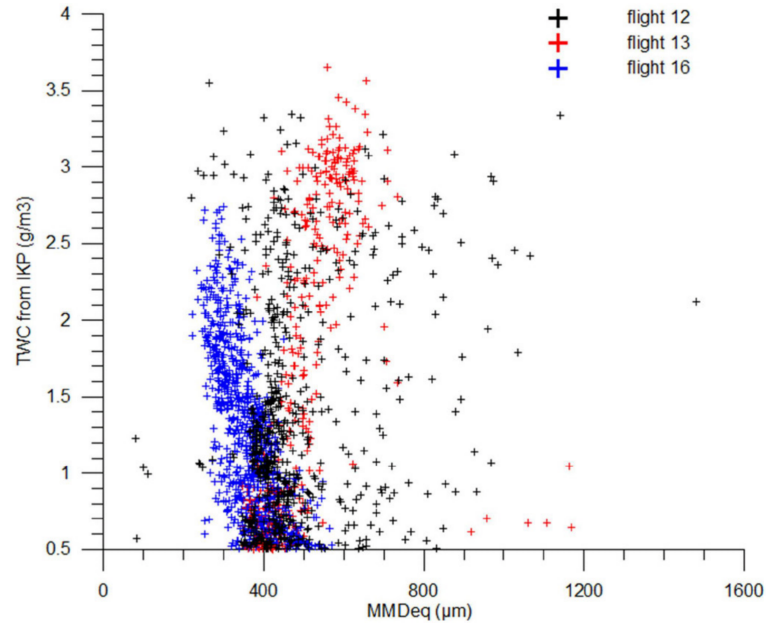


FIGURE 2.2: Scatterplot of the equivalent diameter MDD for ice particles with TWC larger than  $0.5 \text{ g/cm}^3$  for the 3 flights. Figure from [Leroy et al., 2015]

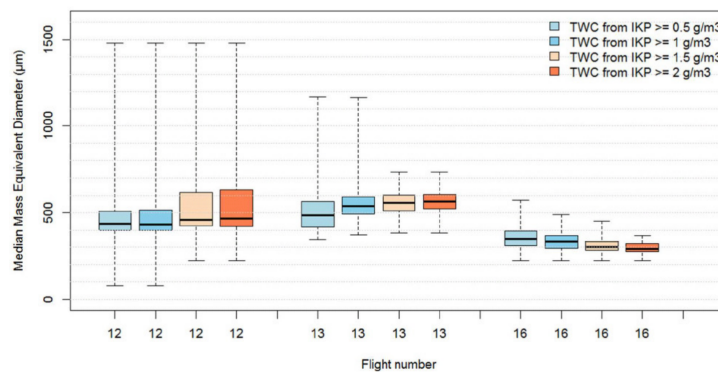


FIGURE 2.3: Boxplot of the distribution of the size of particles for given thresholds of TWC. Figure from Leroy et al. [2015]

[Kintea et al., 2015]. Finally, the different processes that can occur on impact. In normal icing conditions with SLW on a cold substrate, it was assumed that the droplet would freeze on impact. For a SLD there are a lot more possibilities depending on the stage of the ice particle's flight in addition with the state of the substrate. Early on, fragmentation and bouncing of a particle would be expected whereas later, it would be more feasible for sticking to occur. In combination, these provide key inputs when determining the ice accretion.

## 2.3 Experiments

### 2.3.1 Experimental Facilities

The concern over ICI led to the extension of already existing facilities to better represent ICI conditions. Most notable of these are NASA's Propulsion Systems Laboratory unit 3 (PSL-3) at

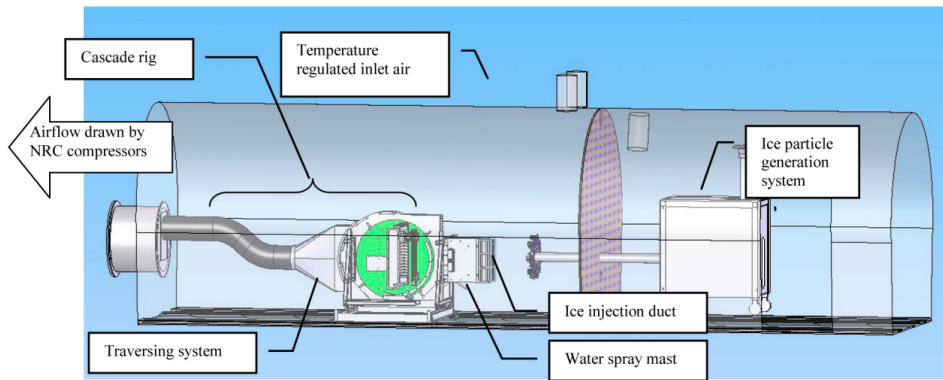


FIGURE 2.4: The RATFac where ice accretion physics research has been performed Currie et al. [2011]. Figure from Currie et al. [2011].

Glenn and the National Research Council of Canada’s (NRCC) Research Altitude Test Facility (RATFac). Over the last decade, most of the large scale experiments have been conducted at these facilities with the PSL-3 being more engine testing orientated whereas the RATFac are for general high altitude conditions. Both of these have been modified to suit this new regime, for example the RATFac can simulate (i) altitudes up to 13.870 m; (ii) temperatures from  $-40\text{ }^{\circ}\text{C}$  to  $35\text{ }^{\circ}\text{C}$ ; (iii) Mach numbers ranging from 0.15 to 0.8; and (iv) IWC up to  $10\text{ g/m}^3$  [NRCC, 2019].

The ice tunnel installed in RATFac by the NRCC is shown in Figure 2.4 [Currie et al., 2011]. The test rig is divided by a partition. The right side is where the ice particles are generated and this can be adjusted to control the mass flow and size of the ice particles. These are then injected through the duct to the warm side of the test cell. With a warmer temperature on the left side, this leads to the ice partially melting creating mixed phase conditions. The water spray mast also also for a liquid water stream in order to increase LWC if desired.

Of course, other facilities exist over the world, but these are more constrained in the experiments that can be done. For example, the TU Braunschweig Icing Wind Tunnel.

### 2.3.2 Prior Experiments

A joint study by Boeing, NASA and NRC in 2009 [Mason et al., 2011] proved that no accretion would occur with ice and surface below freezing temperature. However, it was shown that ice accretion would occur with a warmer than freezing air temperature. Following this, a series of experiments were performed by Currie et al. [2011, 2012, 2013, 2014], Currie and Fuleki [2015] providing the basis for our current understanding of the effect of the LWC/TWC ratio and motivated the idea of a sticking efficiency for ice particles. Figure 2.5 shows the accretion growth on a cylindrical test object.

In addition the experiments comprise the data set from which many new models are tested, for example validation of the IGLOO2D by Trontin and Villedieu [2018]. Experiments by Baumert et al. [2018] continued to examine correlations between sticking efficiency and Mach number as well as accretion shape and growth rate . Later in 2018, the Oxford Thermofluids group led some experiments on the accretion on a gas turbine compressor stator vane, where an example is shown in Figure 2.6. This was done in the RATFac and studies were done for different

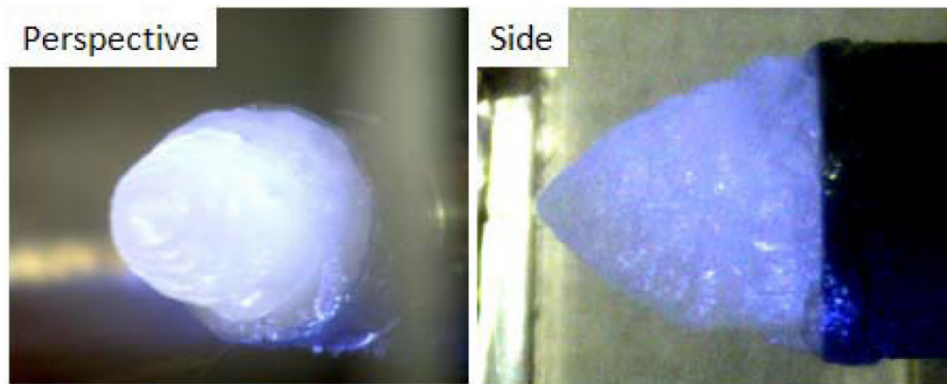


FIGURE 2.5: Accretion growth of a cylindrical test article as performed by Currie and Fuleki [2015] showing both the perspective and side view. Figure from Currie and Fuleki [2015].

diameters of ice, humidity levels, TWC, Mach number as well as angles of incidence [Bucknell et al., 2019b].

## 2.4 Icing models and codes

In order to simulate the results from the experimental facilities, different models and codes have been developed over the years. Beginning with those first developed by the Office National d'Etudes et de Recherches Aéropatiales (ONERA), NASA's Lewis Research Centre and the Royal Aircraft Establishment (RAE) in order to account for SLW, the last fifteen years has seen a new wave of development in order to account for ICI. Many of the numerical models have the same key components of (i) flowfield; (ii) tracking particles; (iii) thermodynamics accretion model on different panels; (iv) accretion profile. The tracking of particles are typically done by a Eulerian or Lagrangian approach whereas the accretion model is usually done on some adaptation of the MM or EMM.

A paper by Mazzawy [2007] highlighted the deficiencies of existing code when it came to mixed/glaciated conditions such as the melting/sticking of ice particles. A NASA report by Wright et al. [2008] came to the same conclusion when testing the codes GlennICE and LEWICE. Moving forward, Wright et al. [2010] had adapted the GlennICE code originally made in 1999. Three modifications were undertaken which are as follows:

- (i) Accounting for a particles energy transfer during flight;
- (ii) Modelling additional processes for mixed phase/glaciated conditions such as erosion;
- (iii) Modifying the energy balance for ice particles impinging on the surface.

Over the last decade, many different groups have been adapting previously existed models while implementing new features. Work was presented by Oliver [2013] based on the Tribus-Messinger Model which is essentially an energy balance of the form:

$$\dot{Q}_{surface} = \dot{Q}_{convection} + \dot{Q}_{latent} + \dot{Q}_{sensible} - \dot{Q}_{kinetic} - \dot{Q}_{friction} \quad (2.1)$$

The full set of energy transfer modes are shown in Figure 2.7 which correspond to the set considered by Tribus [1949] and used by Oliver [2013]. He adapted this model to incorporate ambient humidity and the incoming droplet temperature as a function of the ambient temperature

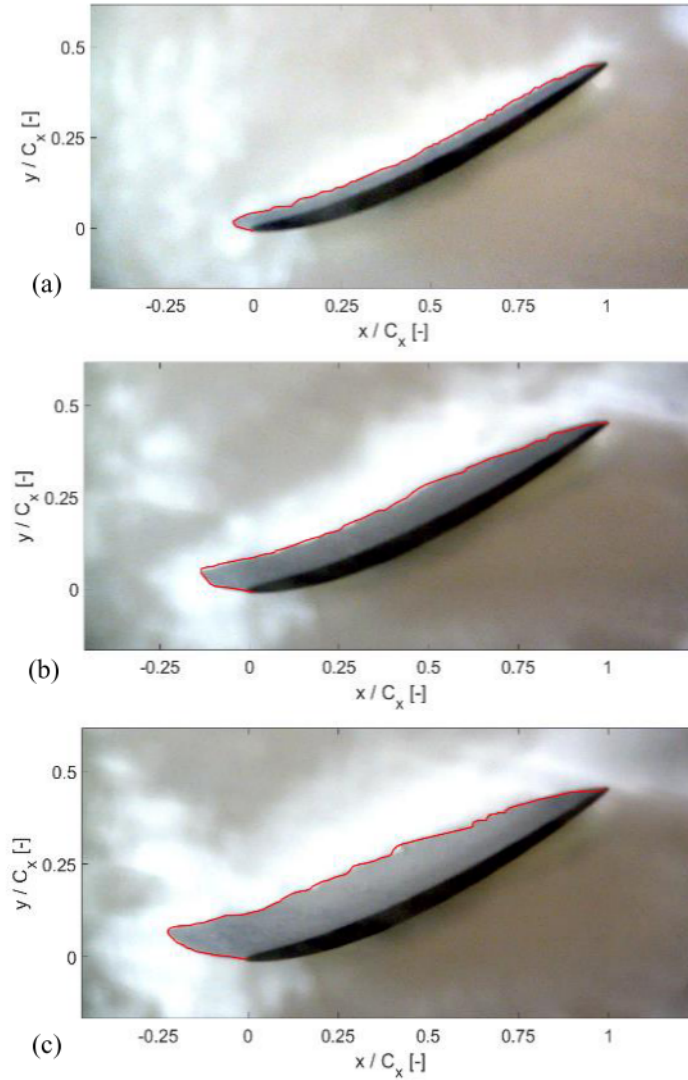


FIGURE 2.6: Experiment performed by [Bucknell et al. \[2019b\]](#) showing the ice accretion at different stages of the experiment. Different stages are (a) 33% of duration; (b) 66%; (c) end of test. The TWC =  $4 \text{ g/m}^3$ . Figure from [Bucknell et al. \[2019b\]](#)

and pressure which was motivated by the NASA and NRCC joint research. The energy balance identifies when  $\dot{Q}_{surface} = 0$  and from the different energy terms outputs the equilibrium surface temperature parameters. The computer model flow chart he used is shown in [Figure 2.8](#).

2017 saw the completion of ONERA's IGLOO2D by [Trontin and Villedieu \[2018\]](#). Its key components are shown in [Figure 2.9](#) where we observe that the numerical tool calculates core aspects such as the aerodynamical flow field in AERO2D, the trajectory of different particles using either an Eulerian or Lagrangian approach as well as an "ice crystal sticking efficiency  $\varepsilon_s$ " in TRAJ2D and finally the accretion solve in ACCRET2D.

The ACCRET2D takes on another adaption of the MM. In their model it accounts for the presence of ice crystals and allows the possibility of water trapped within the ice layer. The Messinger mass balance is written in the form

$$\begin{cases} \dot{m}_{acc}^S + \dot{m}_{Mess}^L = \dot{m}_{rbi} + \dot{m}_{dep} - \dot{m}_{evs} - \dot{m}_{er}, \\ \dot{m}_{Mess}^L = \dot{m}_{acc}^L + \dot{m}_{rbo}, \end{cases} \quad (2.2)$$



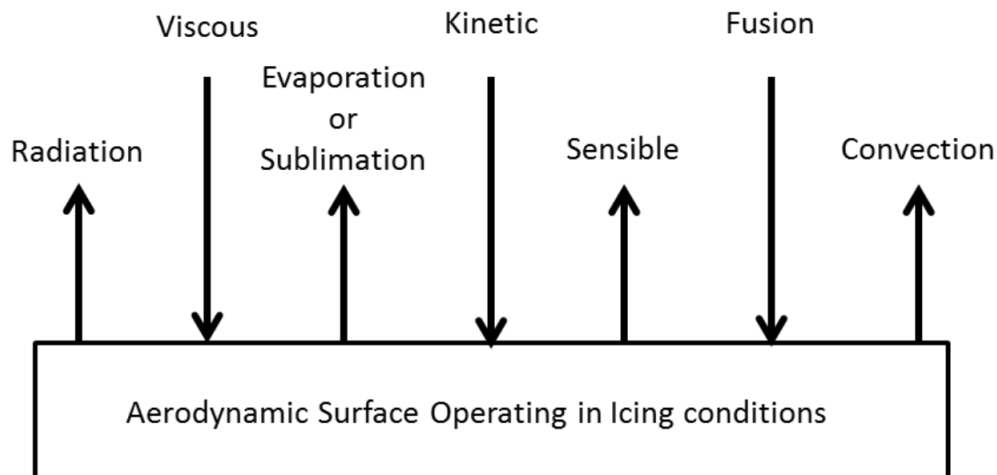


FIGURE 2.7: Set of energy transfer modes considered by Tribus [1949]. Figure from Oliver [2013]

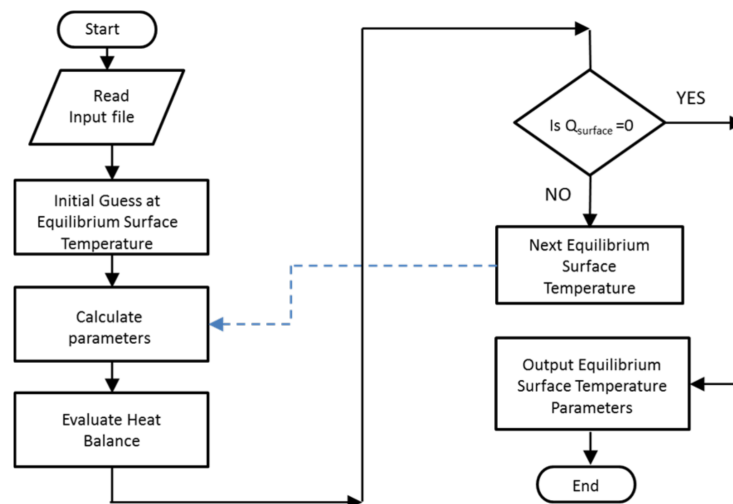


FIGURE 2.8: Flow chart of the MTM code. Figure from [Oliver, 2013].

where the different terms are shown in Figure 2.10. The sticking efficiency calculated in the TRAJ2D gives the proportion of impinging particles that end up depositing.

Finally we examine the work of Bucknell et al. [2019c] from the Oxford Thermofluids group. Motivated by trying to create a new code framework termed ICICLE (Ice Crystal Icing Computational Environment), they developed a three layer thermodynamic model which is an adaptation of the EMM to account for a warm substrate (EMM-ICI). Overall, the ICICLE framework accounted for some of the deficiencies as presented earlier such as (i) including different processes between a particle and a surface - bouncing, fragmentation, etc; (ii) adding two way coupling between the particles and the flow field; in addition to incorporating their new model.

As a result of their new thermodynamic model they proposed the Extended Messinger Model - Crystals (EMM-C) which would use the standard EMM for a cold substrate but their adapted EMM-ICI for a warm one. The model assumes a formation of an initial water layer. If conditions are met such that the top of the layer cools down to the freezing temperature this then allows

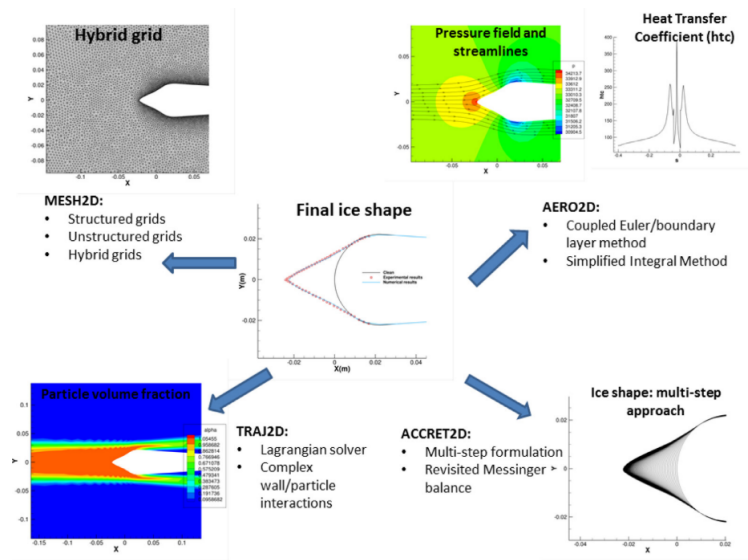


FIGURE 2.9: Overview of the IGLOO2D showing the four main components. Figure from [Trontin and Villedieu, 2018]

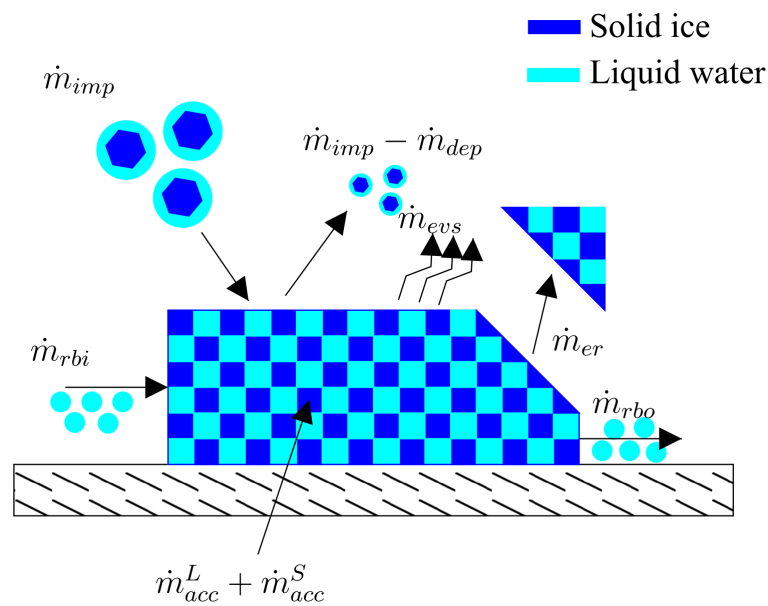


FIGURE 2.10: Different processes in the revisited MM for ICI. Different mass fluxes correspond to impinging ice particles, deposited ice particles, runback water incoming, evaporation, erosion, outgoing runback water and accretion of ice and water trapped within the ice. Figure from [Trontin and Villedieu, 2018].

for the growth of an intermediate ice layer with another thin water layer at the top. This model is discussed more in the new chapter.

**Note 1:** Many other models which have been adapted or developed over the last decade including [Kintea et al. \[2015\]](#) – who change the energy terms so that they would be sources/sinks in the heat equation, [Ayan and Özgen \[2018\]](#) – who adapted the EMM to include solid ice particles in the computations, etc.

**Note 2:** Most of the models in the literature focus on the accretion of ice or the fraction of ice that will stick, it is unclear whether any of them take the breaking off of ice into account.



## Chapter 3

# Three Layer Accretion Model

In 2018 [Bucknell et al. \[2019a\]](#) developed a three layer thermodynamic model which acts as an extension of the work developed by [Myers et al. \[2002\]](#). In this chapter we use the Stefan problem formulation as shown in Section 1.2.2 to create a three layer problem and then reduce the problem at the end to the form as presented by Bucknell.

### 3.1 Formulating the model

In 2002 Myers derived the governing thin film equations for an arbitrary 3D surface from the Navier–Stokes equations. The governing equation was in the form

$$\frac{\partial h}{\partial t} + \nabla_s \cdot \mathbf{Q} = -\frac{\rho_s}{\rho_f} \frac{\partial b}{\partial t} - \mathbf{M} \cdot \mathbf{n} \quad (3.1)$$

where the surface divergence operator is given by

$$\nabla_s \cdot \mathbf{Q} = \frac{1}{(EG)^{1/2}} \left( G^{1/2} \frac{\partial}{\partial s_1} Q_1 + E^{1/2} \frac{\partial}{\partial s_2} Q_2 \right), \quad (3.2)$$

along with the fluid fluxes

$$Q_1 = \int_b^{b+h} u d\eta = - \left( \frac{1}{E^{1/2}} \frac{\partial p}{\partial s_1} - B \mathbf{g} \cdot \mathbf{e}_1 \right) \frac{h^3}{3} + A_1 \frac{h^2}{2}, \quad (3.3)$$

$$Q_2 = \int_b^{b+h} v d\eta = - \left( \frac{1}{G^{1/2}} \frac{\partial p}{\partial s_2} - B \mathbf{g} \cdot \mathbf{e}_2 \right) \frac{h^3}{3} + A_2 \frac{h^2}{2}, \quad (3.4)$$

and pressure given by:

$$p = p_0 - C' \sigma (\kappa_1 + \kappa_2 + \varepsilon(b+h)(\kappa_1^2 + \kappa_2^2)) + \varepsilon \left[ \frac{1}{E} \frac{\partial^2}{\partial s_1^2} (b+h) + \frac{1}{G} \frac{\partial^2}{\partial s_2^2} (b+h) \right]. \quad (3.5)$$

The height  $b$  represents the ice layer whereas  $h$  corresponds to the water layer,  $A_1, A_2$  correspond to shear stresses,  $B$  is the bond number,  $\sigma$  is the surface tension and  $C'$  is the inverse capillary number. In this formulation given by Myers we have  $E, G$  representing the first fundamental forms and  $s_1, s_2$  the directions of principal curvature. The principal curvatures  $\kappa_1, \kappa_2$  are given by  $\kappa_1 = \frac{L}{E}, \kappa_2 = \frac{N}{G}$  where  $L, N$  are the second fundamental forms. . More detail on the differential geometry is found in Appendix 7.

We now present the case in Bucknell which considers a warm substrate. The underlying premise is that initially the flux of water and ice will impinge on the surface, melt and form a water layer. In the case where the energy from the latent heat of fusion is not balanced, then the system loses heat and eventually the surface will be at freezing temperature. At this stage, the three layer model comes into effect.

**Note 1:** For this section we change the notation used by both Myers and Bucknell. Instead of using  $h, b$  to denote the heights of the water and ice layer respectively or  $\theta, T$  for the temperatures of those layers, we instead use  $h_A, h_B, h_C, T_A, T_B, T_C$  where  $A$  corresponds to layer closest to the substrate,  $B$  to the layer on top of  $A$  and use  $h_i, T_i$  for the height and temperature of the  $i^{\text{th}}$  layer for  $i = A, B, C$ .

Looking again at Equation 3.1 for a 1D case with no ice growth on a warm substrate, we end up with

$$\frac{\partial h_A}{\partial t} = \dot{m}_A(t). \quad (3.6)$$

**Note 2:** Again we deviate from the Myers notation and replace  $-\mathbf{M} \cdot \mathbf{n}$  with  $\dot{m}_A$ , where  $\dot{m}_A$  denotes an incoming mass flux.

The water temperature profile is then given by the heat equation

$$\frac{\partial^2 T_A}{\partial z^2} = \frac{c_w \rho_w}{k_w} \frac{\partial T_A}{\partial t} \quad (3.7)$$

where  $c_w$  is the specific heat,  $k_w$  is thermal conductivity and  $\rho_w$  is the density of water. To finish off the system we assume that the substrate is at a constant temperature greater than the freezing temperature, there is initially no water growth and there is a heat flux boundary condition

$$T(0, t) = T_{subs}, \quad h_A(0) = 0 \quad (3.8)$$

$$-k_w \frac{\partial T_A}{\partial z} = q_{loss} - q_{gain}, \quad z = h_A(t), \quad t > 0. \quad (3.9)$$

Here,  $q_{loss}, q_{gain}$  comprise of different mechanisms such as evaporation, convection, particle impinging, kinetic, freezing and so on. The nature of these heat terms are mostly known, however they are defined differently in Oliver [2013], Ayan and Özgen [2018], Brakel et al. [2007], Bucknell et al. [2019a].

In the case where the water surface temperature reaches zero at a critical time  $t^*$ , then we expect to go to phase 2 which is the three layer model. We model this based on a three-phase Stefan problem as discussed in Section 1.2.2 but with an incoming mass flux.

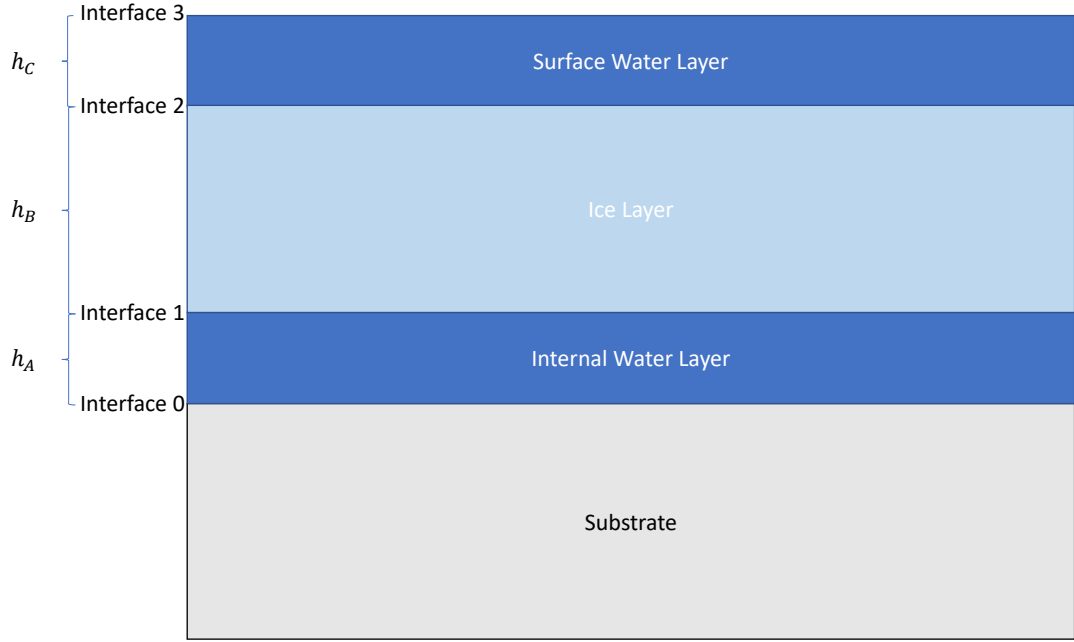


FIGURE 3.1: Schematic for the three layer model depicting the different heights and interfaces.

$$\begin{aligned}
 & \left. \begin{aligned}
 c_w \rho_w \frac{\partial T_A}{\partial t} &= k_w \frac{\partial^2 T_A}{\partial z^2}, & 0 < z < h_A(t) \\
 c_i \rho_i \frac{\partial T_B}{\partial t} &= k_i \frac{\partial^2 T_B}{\partial z^2}, & h_A(t) < z < h_A(t) + h_B(t) \\
 c_w \rho_w \frac{\partial T_C}{\partial t} &= k_w \frac{\partial^2 T_C}{\partial z^2}, & h_A(t) + h_B(t) < z < h_A(t) + h_B(t) + h_C(t)
 \end{aligned} \right\} \text{Heat Equations} \\
 & \left. \begin{aligned}
 L \rho_w \frac{dh_A}{dt} &= k_i \frac{\partial T_B}{\partial z} - k_w \frac{\partial T_A}{\partial z}, & z = h_A(t) \\
 T_A(h_A, t) &= T_B(h_A, t) = T_f \\
 L \rho_i \frac{dh_B}{dt} &= k_w \frac{\partial T_C}{\partial z} - k_i \frac{\partial T_B}{\partial z} + F(t), & z = h_B(t) \\
 T_B(h_A(t) + h_B(t), t) &= T_C(h_A(t) + h_B(t), t) = T_f
 \end{aligned} \right\} \text{Stefan Conditions} \\
 & \left. \begin{aligned}
 h_A(0) &= h_A(t^*), & h_B(0) &= 0, & h_C(0) &= 0 \\
 T_A(z, 0) &= T(z, t^*), & T_B(z, 0) &= 0, & T_C(z, 0) &= 0 \\
 T_A(0, t) &= T_{subs}
 \end{aligned} \right\} \text{Initial Conditions} \\
 & \left. \begin{aligned}
 \frac{\partial T_C}{\partial z} &= q_2(t) - r_2(t) T_C(z, t), & z &= h_A(t) + h_B(t) + h_C(t)
 \end{aligned} \right\} \text{Boundary Conditions} \\
 & \left. \begin{aligned}
 \dot{m}_C &= \rho_w \frac{dh_A}{dt} + \rho_i \frac{dh_B}{dt} + \rho_w \frac{dh_C}{dt}.
 \end{aligned} \right\} \text{Conservation of Mass}
 \end{aligned}$$

## 3.2 Nondimensionalisation

We use tildes for dimensional quantities. We assume that at  $\tilde{t} = 0$ , there is a water layer of height  $\tilde{z} = \tilde{h}_A(\tilde{t})$  on a hot substrate. The water temperature,  $\tilde{T}_A$ , cools to  $\tilde{T}_A = \tilde{T}_{\text{ref}}$  at a critical time  $\tilde{t} = \tilde{t}^*$ , at which point additional ice and water layers,  $\{\tilde{h}_B, \tilde{T}_B\}$  and  $\{\tilde{h}_C, \tilde{T}_C\}$  are introduced.

The system is non-dimensionalised according to

$$\begin{aligned}\tilde{h}_i &= Lh_i \quad \text{and} \quad \tilde{z} = Lz, \\ (\tilde{T}_i) &= \Delta T(T_i) + T_{\text{ref}} \\ \tilde{t} &= [t]t,\end{aligned}$$

where  $i = A, B$  or  $C$ ,  $\Delta T = T_{\text{subs}} - T_f$  is the dimensional difference between substrate temperature and freezing temperature, and  $T_{\text{ref}} = T_f$ . We shall choose the reference length,  $L$  and time,  $[t]$  later.

### 3.2.1 Initial evolution of the water layer

We have the following evolution equations

$$\frac{dh_A}{dt} = \mathcal{M}_A \dot{m}_A(t), \quad (3.10)$$

$$\text{Pe}_w \frac{\partial T_A}{\partial t} = \frac{\partial^2 T_A}{\partial z^2}. \quad (3.11)$$

to be solved subject to the following initial and boundary conditions:

$$h_A(0) = 0, \quad (3.12)$$

$$T_A(0, t) = 1, \quad t > 0 \quad (3.13)$$

$$\frac{\partial T_A}{\partial z} = \mathcal{Q}\{q_1(t) - r_1(t)T_A(z, t)\}, \quad z = h_A(t), \quad t > 0. \quad (3.14)$$

In the above, we have introduced the following non-dimensional quantities:

$$\mathcal{M}_A = \frac{[\dot{m}_A][t]}{\rho_w L}, \quad \text{Pe}_w = \frac{c_w \rho_w L^2}{k_w [t]}, \quad \mathcal{Q} = \frac{L[q]}{k_w \Delta T}, \quad (3.15)$$

where  $c_w$  is specific heat,  $k_w$  is thermal conductivity,  $\rho_w$  is density, and we have introduced a dimensional reference scaling for  $[q_1] = [q] = [r_1]/\Delta T$ . Note that our choice of the functional form on the heat flux condition (3.14) is motivated by the fact that physical flux for the problem considered divides between purely time-dependent forcing (from the external field) and forcing proportional to the temperature (e.g. convection).

**Note 1:** The choice of reference scale for the mass flux,  $[\dot{m}_A]$ , and heat flux,  $\mathcal{Q}$ , is ambiguous until we can provide more information on the functional form of the forcing,  $\dot{m}_A(t)$  and  $q_1(t), r_1(t)$ . In other words, in a numerical simulation, we would choose “arbitrary” values for the combination  $\mathcal{M}_A \dot{m}_A(t)$  and  $\mathcal{Q}q_1, \mathcal{Q}r_1$ —unless we know more information.



**Note 2:** We could have chosen our length scale,  $L$ , and time scale,  $[t]$ , so as to reduce the parameters in the problem. E.g. choose  $L$  such that  $\mathcal{Q} \equiv 1$  and choose  $[t]$  such that  $[\mathcal{M}_A] \equiv 1$ . However we leave things general for now.

### 3.2.2 Three Layer Model

We thus solve the single-layer water problem until  $T_A = 0$  at some critical time,  $t = t^*$ , and then solve the three-layer problem presented in this section. The main difference in the three-layer model is the consideration of the moving ice interface, which, for a surface  $z = h(t)$ , is governed by a Stefan boundary condition. In dimensional form, this appears as

$$\rho_i La \frac{dh_i}{dt} = k_w \frac{\partial \tilde{T}_w}{\partial \tilde{z}} - k_i \frac{\partial \tilde{T}_i}{\partial \tilde{z}} + \text{sources/sinks}, \quad (3.16)$$

where  $La$  is the latent heat of water for the phase exchange to/from ice ( $La \approx 3 \times 10^5 \text{J/kg}$ ). This motivates the definition of the Stefan number,  $St$ , defined by

$$St = \frac{\rho_i L^2 La}{k_i \Delta T [t]} \quad (3.17)$$

The set of governing non-dimensional equations for the three-layer problem is then given by the heat equation for each layer with

$$\frac{\partial^2 T_A}{\partial z^2} = \text{Pe}_w \frac{\partial T_A}{\partial t}, \quad T_A(0, t) = 1, \quad T_A(h_A, t) = 0 \quad (3.18)$$

$$\frac{\partial^2 T_B}{\partial z^2} = \text{Pe}_i \frac{\partial T_B}{\partial t}, \quad T_B(h_A, t) = 0, \quad T_B(h_A + h_B, t) = 0 \quad (3.19)$$

$$\frac{\partial^2 T_C}{\partial z^2} = \text{Pe}_w \frac{\partial T_C}{\partial t}, \quad T_C(h_A + h_B, t) = 0, \quad \frac{\partial T_C}{\partial z} = Q\{q_2 - r_2 T_C(z, t)\}, \quad z = h_A(t) + h_B(t) + h_C(t) \quad (3.20)$$

in addition to the equations for the height growth

$$\frac{dh_A}{dt} + \frac{\rho_i}{\rho_w} \frac{dh_B}{dt} + \frac{dh_C}{dt} = \mathcal{M}_C \dot{m}_C(t), \quad (3.21)$$

$$S_w \frac{dh_A}{dt} = \frac{k_i}{k_w} \frac{\partial T_B}{\partial z} - \frac{\partial T_A}{\partial z}, \quad z = h_A \quad (3.22)$$

$$S_i \frac{dh_B}{dt} = \frac{k_w}{k_i} \frac{\partial T_C}{\partial z} - \frac{\partial T_B}{\partial z} + \mathcal{F} \quad z = h_A + h_B \quad (3.23)$$

$$h_A(0) = h_A(t^*) \quad (3.24)$$

$$h_B(0) = 0 \quad (3.25)$$

$$h_C(0) = 0 \quad (3.26)$$

where  $\mathcal{F}$  refers to any sources or sinks as described above. We use the same non dimensionalisation as used in the single-layer problem. In similar fashion, we introduce the following non-dimensional

quantities for the three-layer problem:

$$\mathcal{M}_C = \frac{[\dot{m}_C][t]}{\rho_w L}, \quad \text{Pe}_w = \frac{c_w \rho_w L^2}{k_w [t]}, \quad \text{Pe}_i = \frac{c_i \rho_i L^2}{k_i [t]}, \quad (3.27)$$

$$Q = \frac{L[\hat{q}]}{k_w \Delta T}, \quad \text{St}_w = \frac{\rho_w L^2 La}{k_w \Delta T [t]}, \quad \text{St}_i = \frac{\rho_i L^2 La}{k_i \Delta T [t]}, \quad (3.28)$$

**Note 1:** We expect that many of the fluxes composing  $q_2, r_2$  in addition to  $\dot{m}_C$  to be similar to that of the single-layer problem. However, with the formation of the ice layer, it is no longer necessary for all incoming ice particles to melt. Some may penetrate the thin water layer and thus be considered as a source in the stefan condition.

**Note 2:** The change in height of the ice layer  $h_B$  can be split into two components: the freezing or melting of the top and bottom interface. Thus we can write  $\frac{dh_B}{dt} = \frac{dh_{B,AB}}{dt} + \frac{dh_{B,BC}}{dt}$ , where the first term corresponds to changes on the interface between the first and second layers while the second is for the middle ice layer and the top water layer.

### 3.3 Bucknell Reduction

For the single water layer, Bucknell writes the incoming mass flux in terms of the different contributions

$$\dot{m}_A = \dot{m}_{stuck,i} + \dot{m}_{stuck,w} + \dot{m}_{run,in} - \dot{m}_{evap} \quad (3.29)$$

In this stage it is assumed that all the incoming ice particles must melt. However when moving to the three layer phase is no longer assumed. Firstly Bucknell assumes the top water layer is sufficiently thin. This results in both ice particle penetrating the water layer and sticking and also that wall temperature gradients are neglected for the surface water layer. As we have done, he splits the ice growth into internal and surface as above resulting in

$$\frac{dh_A}{dt} + \frac{\rho_i}{\rho_w} \frac{dh_{B,AB}}{dt} = 0, \quad (3.30)$$

$$\rho_i \frac{dh_{B,BC}}{dt} + \rho_w \frac{dh_C}{dt} = \dot{m}_C \quad (3.31)$$

He then further splits Equation 3.31 into different components which affect the water layer and the ice layer separately in addition to a freezing flux which adds to the ice layer from the water layer [Bucknell et al., 2019a].

$$\rho_w \frac{dh_C}{dt} = \dot{m}_{stuck,w} + \dot{m}_{run,in} - \dot{m}_{evap} - \dot{m}_{freeze}, \quad (3.32)$$

$$\rho_i \frac{dh_{B,BC}}{dt} = \dot{m}_{stuck,i} + \dot{m}_{freeze}. \quad (3.33)$$

In order to calculate the  $\dot{m}_{freeze}$  term, he examines what we would take to be the top surface boundary condition. Given his assumption that  $T_C = 0$ , this results in

$$\frac{\partial T_C}{\partial z} = q_{loss} - q_{gain}, \quad z = h_A + h_B + h_C, \quad (3.34)$$

$$0 = q_{loss} - q_{gain}, \quad z = h_A + h_B + h_C, \quad (3.35)$$

and so by balancing these heat terms, he finds the fraction that freezes. In practise, he removes the second Stefan equation and essentially replaces it with the normal Messinger heat balance.



## Chapter 4

# An extended look into the Three Layer Thermodynamic Model

This chapter examines the three layer thermodynamic model as presented in the previous chapter.

### 4.1 Asymptotic behaviour for small Peclet number

#### 4.1.1 Water Layer

Our system for the single water layer is described by the Equations 3.10 – 3.11 introduced in the previous section. We end up writing  $\mathcal{M}_A \dot{m}_A(t) = J(t)$  for ease and our BCs for the heat equation are given by Equations 3.12 – 3.14. Let  $\text{Pe} \ll 1$  assuming a quasi-steady state for our system, we then write our temperature as an expansion of increasing orders of the Peclet number.

$$T_A = T_A^{(0)} + \text{Pe}_w T_A^{(1)} + \dots$$

Starting with the continuity equation we get

$$\frac{dh_A}{dt} = J(t), \quad (4.1)$$

which can be integrated to give  $h_A = \int_0^t J(s) ds$ .

Rewriting the heat equation in terms of this expansion yields

$$\text{Pe}_w \frac{\partial T_A^{(0)}}{\partial t} + \text{Pe}_w^2 \frac{\partial T_A^{(1)}}{\partial t} + \dots = \frac{\partial^2 T_A^{(0)}}{\partial z^2} + \text{Pe}_w \frac{\partial^2 T_A^{(1)}}{\partial z^2} + \dots \quad (4.2)$$

At order  $\text{Pe}_w^0$  we have

$$\frac{\partial^2 T_A^{(0)}}{\partial z^2} = 0,$$

which can be solved to give

$$T_A^{(0)} = a(t)z + b(t).$$

Subbing in the first boundary condition gives us  $b(t) = 1$ . Examining our heat flux boundary condition, we can rewrite in terms of our expansion as

$$\left. \frac{\partial T_A^{(0)}}{\partial z} \right|_{z=h_A(t)} + \text{Pe} \left. \frac{\partial T_A^{(1)}}{\partial z} \right|_{z=h_A(t)} + \dots = \mathcal{Q}\{q_1 - r_1[T_A^{(0)}(h_A(t)) + \text{Pe} T_A^{(1)}(h_A(t)) + \dots]\} \quad (4.3)$$

At Peclet order 0, we have:

$$\left. \frac{\partial T_A^{(0)}}{\partial z} \right|_{z=h_A(t)} = \mathcal{Q}\{q_1 - r_1[T_A^{(0)}(h_A(t))]\} \quad (4.4)$$

$$a(t) = \mathcal{Q}\{q_1 - r_1(a(t)h_A(t) + 1)\} \quad (4.5)$$

$$a(t) = \frac{\mathcal{Q}(q_1 - r_1)}{1 + \mathcal{Q}r_1h_A(t)}, \quad (4.6)$$

so we can write  $T_A^{(0)} = \frac{\mathcal{Q}(q_1 - r_1)}{1 + \mathcal{Q}r_1h_A(t)}z + 1$ . From the heat equation, at Peclet order 1 we have

$$\frac{\partial T_A^{(0)}}{\partial t} = \frac{\partial^2 T_A^{(1)}}{\partial z^2} \quad (4.7)$$

Taking the time derivative of  $T_A^{(0)}$  we get

$$-\frac{\mathcal{Q}^2 r_1 (q_1 - r_1)}{(1 + \mathcal{Q}r_1h_A(t))^2} J(t)z = \frac{\partial^2 T_A^{(1)}}{\partial z^2}. \quad (4.8)$$

Integrating twice gives

$$T_A^{(1)} = -\frac{\mathcal{Q}^2 r_1 (q_1 - r_1)}{6(1 + \mathcal{Q}r_1h_A(t))^2} J(t)z^3 + c(t)z + d(t), \quad (4.9)$$

where from our initial condition  $d(t) = 0$ .

From the heat flux boundary condition at Peclet order 1 we have

$$\left. \frac{\partial T_A^{(1)}}{\partial z} \right|_{z=h_A(t)} = -\mathcal{Q}r_1 T_A^{(1)}(h_A(t)), \quad (4.10)$$

$$-\frac{\mathcal{Q}^2 r_1 (q_1 - r_1)}{2(1 + \mathcal{Q}r_1h_A(t))^2} J(t)h_A^2 + c(t) = -\mathcal{Q}r_1 \left( -\frac{\mathcal{Q}^2 r_1 (q_1 - r_1)}{6(1 + \mathcal{Q}r_1h_A(t))^2} J(t)h_A^3 + c(t)h_A \right), \quad (4.11)$$

$$c(t) = \frac{\mathcal{Q}^2 r_1 (q_1 - r_1)}{2(1 + \mathcal{Q}r_1h_A(t))^2} J(t)h_A(t)^2 \left( \frac{3 + \mathcal{Q}r_1h_A(t)}{1 + \mathcal{Q}r_1h_A(t)} \right). \quad (4.12)$$

This gives us our first order correction of

$$T_A^{(1)} = -\frac{\mathcal{Q}^2 r_1 (q_1 - r_1)}{6(1 + \mathcal{Q}r_1h_A(t))^2} J(t)z^3 + \frac{\mathcal{Q}^2 r_1 (q_1 - r_1)}{2(1 + \mathcal{Q}r_1h_A(t))^2} J(t)h_A(t)^2 \left( \frac{3 + \mathcal{Q}r_1h_A(t)}{1 + \mathcal{Q}r_1h_A(t)} \right) z. \quad (4.13)$$

Our temperature profile is thus given as

$$T_A = \frac{\mathcal{Q}(q_1 - r_1)}{1 + \mathcal{Q}r_1 h_A(t)} z + 1 + \text{Pe}_w \left[ -\frac{\mathcal{Q}^2 r_1 (q_1 - r_1)}{6(1 + \mathcal{Q}r_1 h_A(t))^2} J(t) z^3 + \frac{\mathcal{Q}^2 r_1 (q_1 - r_1)}{2(1 + \mathcal{Q}r_1 h_A(t))^2} J(t) h_A(t)^2 \left( \frac{3 + \mathcal{Q}r_1 h_A(t)}{1 + \mathcal{Q}r_1 h_A(t)} \right) z \right]. \quad (4.14)$$

#### 4.1.2 Three Layer model

Starting with the layout template given by Figure 3.1 we have the full set of nondimensional equations for the 3 layer system.

At order  $\text{Pe}_w^0$  we start with the temperature of the internal water. At this order, we have  $\frac{\partial^2 T_A^{(0)}}{\partial z^2} = 0$  with BC given by Equation 3.18. Using these we get  $T_A^{(0)} = -\frac{z}{h_A} + 1$ .

We then have the temperature of the ice layer given trivially by  $T_B = 0$ . Substituting these into the Stefan equation for the  $AB$  interface gives

$$\text{St}_w \frac{dh_A}{dt} = -\frac{-1}{h_A} \quad (4.15)$$

which can be integrated using the initial condition to give  $h_A(t) = \sqrt{h_{A,0}^2 + \frac{2}{\text{St}_w} t}$ .

Examining the temperature of the top layer we have  $T_C^{(0)} = c(t)z + d(t)$ . Applying the first initial condition gives that  $d(t) = -c(t)[h_A + h_B]$ . The heat flux boundary condition is then given by

$$\left. \frac{\partial T_C^{(0)}}{\partial z} \right|_{h_A+h_B+h_C} = \mathcal{Q}(q_2 - r_2 T_C^{(0)}(h_A + h_B + h_C))$$

where, upon solving gives  $T_C^{(0)} = \frac{\mathcal{Q}q_2}{1 + \mathcal{Q}r_2 h_C} [z - h_A - h_B]$ .

The growth of the ice layer is given by the contribution of both the melting/freezing on its top/bottom surface. Adding the two components gives

$$\frac{dh_B}{dt} = -\frac{\rho_w}{\rho_i} \frac{dh_A}{dt} + \frac{1}{\text{St}_i} \left[ \frac{k_w}{k_i} \left. \frac{\partial T_C^{(0)}}{\partial z} \right|_{z=h_A+h_B} + \mathcal{F} \right], \quad (4.16)$$

$$= -\underbrace{\frac{\rho_w}{\rho_i} \frac{dh_A}{dt}}_{\frac{dh_{B,AB}}{dt}} + \underbrace{\frac{1}{\text{St}_i} \left[ \frac{k_w}{k_i} \frac{\mathcal{Q}q_2}{1 + \mathcal{Q}r_2 h_C} + \mathcal{F} \right]}_{\frac{dh_{B,BC}}{dt}} \quad (4.17)$$

Integration gives

$$h_B(t) = h_{B,0} - \frac{\rho_w}{\rho_i} \left[ \sqrt{h_{A,0}^2 + \frac{2}{\text{St}_w} t} - h_{A,0} \right] + \frac{1}{\text{St}_i} \int_0^t \left[ \frac{k_w}{k_i} \frac{\mathcal{Q}q_2(s)}{1 + \mathcal{Q}r_2(s)h_C(s)} + \mathcal{F} \right] ds.$$

Finally, to get the height of the top fluid layer we look at the conservation of mass. Having split the ice layer into the two components as done in Note 2 in the previous section we have

$$\frac{dh_C}{dt} = -\frac{\rho_i}{\rho_w} \frac{dh_{B,BC}}{dt} + \mathcal{M}_C \dot{m}_C \quad (4.18)$$

and thus

$$\frac{dh_C}{dt} = -\frac{\rho_i}{\rho_w} \frac{1}{St_i} \left[ \frac{k_w}{k_i} \frac{Qq_2}{1 + Qr_2 h_C} + \mathcal{F} \right] + \mathcal{M}_C \dot{m}_C \quad (4.19)$$

we are left with a non-linear equation for  $h_C$  as a function of  $t$  which is no longer trivial to solve. At this stage we note the feedback loop, where the temperature plays a direct role in the growth of the top water layer through the Stefan equation for the ice layer and the conservation of mass, while the height influences the temperature through the boundary condition at the top.

## 4.2 Numerical Methodology of three layer problem

### 4.2.1 Finite Difference of 3 Layer model

We examine the three layer system using a backward differencing scheme. Firstly however we rescale our system. From Figure 3.1 we have our three heights in the system given by:

- $\bar{h}_A = h_A$
- $\bar{h}_B = h_A + h_B$
- $\bar{h}_C = h_A + h_B + h_C$

With our domain is expanding over time as well as the interfaces moving over time, we scale the full system so that  $z = h(t)\xi \rightarrow \xi = \frac{z}{h(t)}$ . We write our temperature profiles in terms of a single temperature which changes with the domain such that:

$$T(z, t) = \begin{cases} T_A, & \text{for } 0 \leq z \leq \bar{h}_A \\ T_B, & \text{for } \bar{h}_A \leq z \leq \bar{h}_B \\ T_C, & \text{for } \bar{h}_B \leq z \leq \bar{h}_C \end{cases} \quad (4.20)$$

We rescale each of our subintervals by

- $z = \xi_1 h_A$  for  $0 < z < \bar{h}_A$ ,
- $z = \xi_1 + \xi_2 h_B$  for  $\bar{h}_A \leq z \leq \bar{h}_B$ ,
- $z = \xi_1 + \xi_2 + \xi_3 h_C$  for  $\bar{h}_B \leq z \leq \bar{h}_C$ .

However, in our system our middle layer is just trivially  $T_B = 0$ . This allows us to tackle the top and bottom layer independently. Let  $T(z, t) = U(\xi, t)$ . Rewriting our PDE for the top and



bottom layer gives:

$$\left. \frac{\partial T}{\partial t} \right|_z = \left. \frac{\partial U}{\partial \xi} \frac{\partial \xi}{\partial t} \right|_t + \left. \frac{\partial U}{\partial t} \right|_\xi = -\frac{z}{h^2} \dot{h} U_\xi + U_t \quad (4.21)$$

$$\left. \frac{\partial T}{\partial z} \right|_t = \frac{1}{h} \left. \frac{\partial U}{\partial \xi} \right|_t = \frac{1}{h} U_\xi \quad (4.22)$$

$$\left. \frac{\partial^2 T}{\partial z^2} \right|_t = \frac{1}{h^2} U_{\xi\xi} \quad (4.23)$$

$$\Rightarrow \frac{1}{h^2} U_{\xi\xi} = Pe \left( U_t - \frac{z}{h^2} U_\xi \right) \quad (4.24)$$

$$Pe U_t = Pe \frac{\xi}{h} U_\xi + \frac{1}{h^2} U_{\xi\xi} \quad (4.25)$$

We adopt the backwards differencing scheme for our second derivative and a central difference for the first spatial derivative. We write these as follows:

$$\frac{\partial U}{\partial t}(\xi_i, t_{n+1}) = \frac{U_i^{n+1} - U_i^n}{\Delta t} + O(\Delta t) \quad (4.26)$$

$$\frac{\partial^2 U}{\partial \xi^2}(\xi_i, t_{n+1}) = \frac{U_{i-1}^{n+1} - 2U_i^{n+1} + U_{i+1}^{n+1}}{\Delta \xi^2} + O(\Delta \xi^2) \quad (4.27)$$

$$\frac{\partial U}{\partial z}(\xi_i, t_n) = \frac{U_{i+1}^n - U_{i-1}^n}{2\Delta \xi} + O(\Delta \xi) \quad (4.28)$$

Here  $n$  refers to the timestep,  $\Delta \xi = \xi_{i+1} - \xi_i$  and  $i$  denotes the space in the grid, where  $2 \leq i \leq N+1$  represent the internal grid points for each layer. Plugging these schemes into the above equation gives us

$$-\frac{\Delta t}{h^2 \Delta \xi^2} U_{i-1}^{n+1} + \left( Pe + \frac{2\Delta t}{h^2 \Delta \xi^2} \right) U_i^{n+1} - \frac{\Delta t}{h^2 \Delta \xi^2} U_{i+1}^{n+1} = -\frac{Pe \Delta t \dot{h} \xi}{2h \Delta \xi} U_{i-1}^n + Pe U_i^n + \frac{Pe \Delta t \dot{h} \xi}{2h \Delta \xi} U_{i+1}^n \quad (4.29)$$

Here  $h = \bar{h}_C$ ,  $\dot{h}$  is the change in the total height with regards to time,  $\xi$  and  $\Delta \xi$  are the space and mesh size in the respective domain. The system we end up solving equates to

$$BU^{n+1} = CU^n + f, \quad (4.30)$$

where  $B, C \in R^{3N \times 3N}$  are the matrices that govern the PDE,  $U^n \in R^{3N}$  is the solution at the  $n^{th}$  time step and  $f \in R^{3N}$  are extra terms that appear due to boundary conditions.

Given the middle layer is just at zero the entire time, this allows us to solve the top and bottom layer independently. This means that we can find the  $B, C \in R^{N \times N}$ ,  $U, f \in R^N$  for the top and bottom layer and solve separately. We therefore allow an internal grid space of  $2 \leq i \leq N+1$  for the bottom layer and  $2N+2 \leq k \leq 3N+1$  for the top layer respectively. The spacing for these grids are different as they scale with  $\xi_1$  and  $\xi_3$ .

**Note:** Although in this case, our middle layer is just zero, for other systems it might not be, so we leave the grid  $N+2 \leq j \leq 2N+1$ .

Using this framework, the boundary conditions for the bottom layer are given by

$$U_1^n = 1 \quad (4.31)$$

$$U_{N+2}^n = 0 \quad (4.32)$$

This first boundary condition is trivially solves so instead of solving for  $N + 1$  equations in  $U$ , we take out this first and add it to  $f$ .

The top layer boundary conditions are given by

$$U_{2N+2}^n = 0 \quad (4.33)$$

$$\frac{U_{3N+2} - U_{3N}}{2\Delta h\xi} = \mathcal{Q}(q_2 - r_2 U_{3N+1}) \quad (4.34)$$

This second boundary condition given by the heat flux can be rearranged as

$$U_{3N+2} = -2\Delta h\xi r_2 U_{3N+1} + U_{3N} + 2\mathcal{Q}q_2\Delta h\xi \quad (4.35)$$

which can then be substituted into the above master equation yielding

$$-\frac{2\Delta t}{h^2\Delta\xi^2}U_{3N}^{n+1} + (\text{Pe} + \frac{2\Delta t}{h^2\Delta\xi^2} + \frac{2\Delta t\mathcal{Q}r_2}{h\Delta\xi})U_{3N+1}^{n+1} = (\text{Pe} - \text{Pe}\Delta t\dot{h}\xi\mathcal{Q}r_2)U_{3N+1}^n + \text{other terms} \quad (4.36)$$

The bottom layer is thus given by

$$\begin{pmatrix} (1+2b_1) & -b_1 & 0 & 0 \\ -b_1 & \ddots & \ddots & 0 \\ 0 & \ddots & \ddots & -b_1 \\ 0 & 0 & -b_1 & (1+2b_1) \end{pmatrix} \begin{pmatrix} u_2^{n+1} \\ \vdots \\ \vdots \\ u_{N+1}^{n+1} \end{pmatrix} = \begin{pmatrix} \text{Pe} & c_1 & 0 & 0 \\ -c_1 & \ddots & \ddots & 0 \\ 0 & \ddots & \ddots & c_1 \\ 0 & 0 & -c_1 & \text{Pe} \end{pmatrix} \begin{pmatrix} u_2^n \\ \vdots \\ \vdots \\ u_{N+1}^n \end{pmatrix} + \begin{pmatrix} p \\ 0 \\ \vdots \\ 0 \end{pmatrix} \quad (4.37)$$

where  $b_1 = -\frac{\Delta t}{h^2\Delta\xi^2}$  and  $c_1 = \frac{\text{Pe}\Delta t\dot{h}\xi}{2h\Delta\xi}$ .

The top water layer is given by

$$\begin{pmatrix} (1+2b_1) & -b_1 & 0 & 0 \\ -b_1 & \ddots & \ddots & 0 \\ 0 & \ddots & (1+2b_1) & -b_1 \\ 0 & 0 & -2b_1 & (1+2b_1+a) \end{pmatrix} \begin{pmatrix} u_{2N+2}^{n+1} \\ \vdots \\ \vdots \\ u_{3N+1}^{n+1} \end{pmatrix} = \begin{pmatrix} \text{Pe} & c_1 & 0 & 0 \\ -c_1 & \ddots & \ddots & 0 \\ 0 & \text{Pe} & c_1 & 0 \\ 0 & 0 & 0 & \text{Pe} \end{pmatrix} \begin{pmatrix} u_{2N+2}^n \\ \vdots \\ \vdots \\ u_{3N+1}^n \end{pmatrix} + \begin{pmatrix} 0 \\ \vdots \\ 0 \\ d \end{pmatrix} \quad (4.38)$$

Here  $b_1, c_1$  are defined as above. In addition we have  $a = \frac{2\Delta t\mathcal{Q}r_2}{h\Delta\xi}$  and  $d = \frac{\Delta t}{h\Delta\xi}\mathcal{Q}q_2 + \text{Pe}\Delta t\dot{h}\xi\mathcal{Q}q_2$ .

Having solved for the temperatures, we use this to update our heights of the different layers. Beginning with the bottom water layer and progressing upwards gives

$$h_A^{k+1} = h_A^k - \Delta t \left( \frac{1}{h} \frac{\partial T_A}{\partial \xi} \right)^{k+1}, \quad (4.39)$$

$$h_B^{k+1} = h_B^k - \frac{1}{P} (h_A^{k+1} - h_A^k) + \frac{\Delta t}{\text{St}_i} \left( K \left( \frac{1}{h} \frac{\partial T_C}{\partial \xi} \right)^{k+1} + \mathcal{F} \right), \quad (4.40)$$

$$h_C^{k+1} = h_C^k - P \frac{\Delta t}{\text{St}_i} \left( K \left( \frac{1}{h} \frac{\partial T_C}{\partial \xi} \right)^{k+1} + \mathcal{F} \right) + \mathcal{M}_C \dot{m}_C \Delta t. \quad (4.41)$$

where  $P = \frac{\rho_i}{\rho_w}$  and  $K = \frac{k_w}{k_i}$ .

### 4.2.2 Simulations

Here we perform some simulations for the transition between the water layer and three layer model. For the simulations, we have set  $\mathcal{Q} = 1$ ,  $q_1 = -0.25$ ,  $r_1 = 1$ ,  $q_2 = 0.25$ ,  $r_2 = 1$ ,  $\mathcal{M}_A \dot{m}_A = 1$ ,  $\mathcal{M}_C \dot{m}_C = 1$ ,  $P = 1$ ,  $K = 0.25$ . We have set  $N = 63$  and  $\Delta t = 10^{-3}$ . We

We have our water layer which grows until  $t^*$  where the surface temperature becomes 0. Then we initialise our three layer sequence, where for our initial conditions we have set  $h_A(0) = h_A(t^*)$ ,  $h_B(0) = 10^{-7}$ ,  $h_C(0) = 10^{-7}$ . We then run for the three layer for a time of  $\bar{t} = 6$ .

In Figures 4.1 and 4.2 our default values are  $Pe_w = 1$ ,  $St_w = 1$ ,  $St_i = 1$ ,  $\mathcal{F} = 0.75$ . Figures on the left represent correspond to the height profile for  $t \in [0, \bar{t} + t^*]$  whereas, those on the right show the temperature profile at  $\bar{t} + t^*$  for the rescaled domain.

**Note:** Our code stops in the case that  $h_B$  or  $h_C$  becomes negative. As such, we have chosen parameters  $Pe, St_w, St_i, \mathcal{F}$  such that  $h_B, h_C \leq 0 \forall t$ .

Firstly we observe that the incoming mass flux is the same for both the single and three layer problem, which results in a linear total height profile. Then by comparing the default set of values with the adjusted parameter we get insight as to how each of these affect the system, both in terms of relative height and also in terms of the temperature profile.

- In Figure 4.1 (c) we observe a much larger ice growth and a small top water layer. From Equations 3.21 and 3.23 this is what we'd intuitively expect.
- In Figure 4.2 (a), for smaller value of  $St_w$  this results in larger changes in height relative to temperature gradient. Thus we'd expect to see a larger internal water layer profile which is what we observe. Note that there is no change in the top water layer's height.
- Figure 4.2 (c), for smaller value of  $St_i$  this results in larger changes in height for the ice layer relative to temperature gradient between the interface 2 and 3. As such we note that there is no change in the internal water layer, but the ice layer has increased in height relative to the top layer.
- Finally in Figure 4.1 (e-f), firstly we notice a more linear temperature profile in f. Changing the Peclet number directly affects the temperature profiles of both  $T_A$  and  $T_C$ , which then feeds into both Stefan equations.

Of special interest is the region  $\bar{t} \in [0, 1]$  as we see how regimes where either the ice layer or the top water layer disappears, can exist.

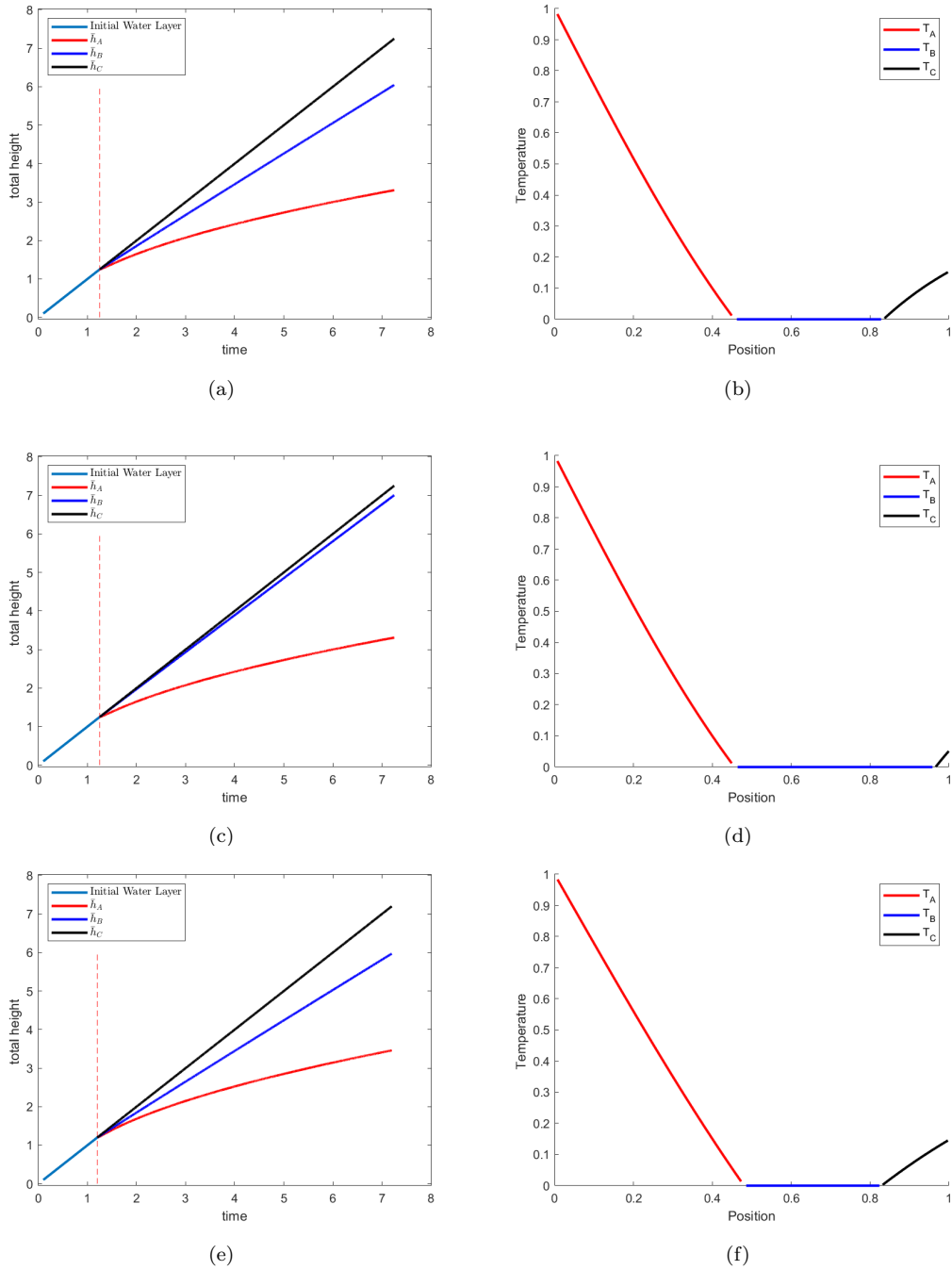


FIGURE 4.1: These plots show the heights (left) and temperatures (right) as a function of time obtained through numerical simulations of the three-layer model. Figures on the left show the height profile for  $t \in [0, \bar{t} + t^*]$ . Those on the right show the temperature profile at  $\bar{t} + t^*$ . We use default values of  $Pe_w = 1$ ,  $St_w = 1$ ,  $St_i = 1$ ,  $\mathcal{F} = 0.75$  for insets (a) and (b). Inset (c) and (d) uses the same values but with  $\mathcal{F} = 0.9$ . Similarly insets (e) and (f) use  $Pe = 0.25$ .

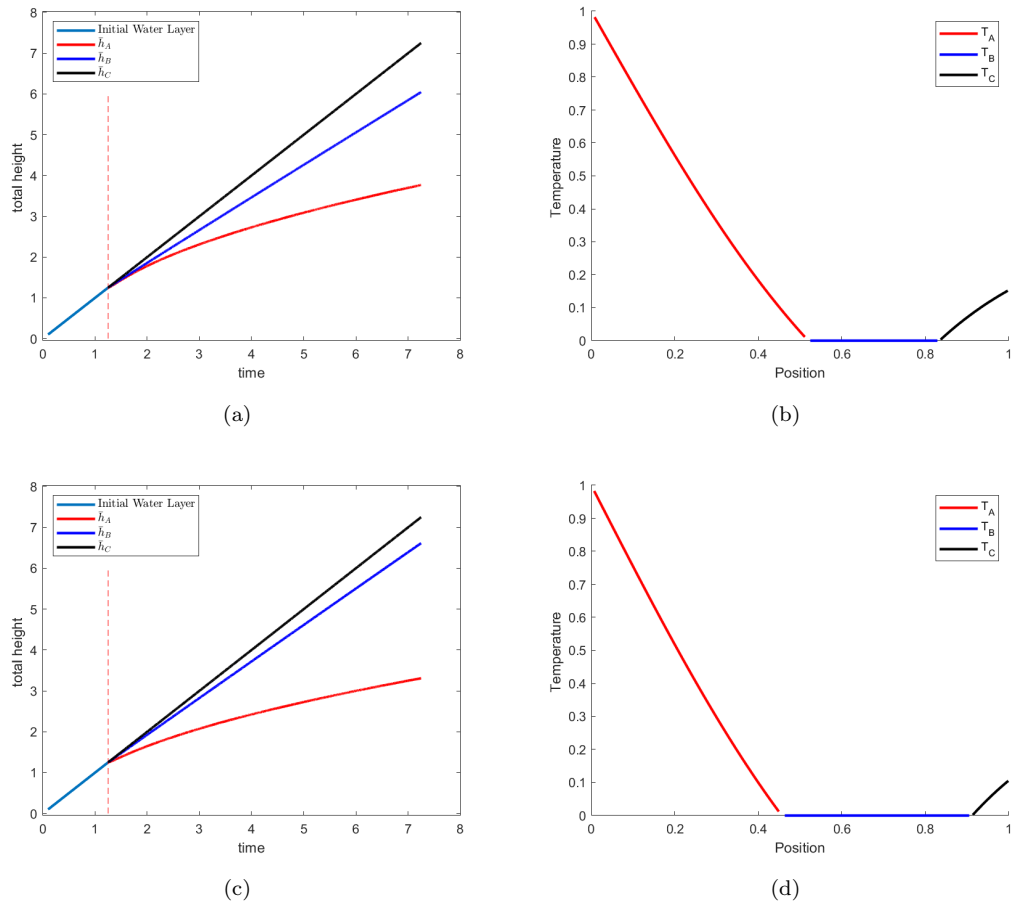


FIGURE 4.2: These plots show the heights (left) and temperatures (right) as a function of time obtained through numerical simulations of the three-layer model. Figures on the left show the height profile for  $t \in [0, \bar{t} + t^*]$ . Those are the right show the temperature profile at  $\bar{t} + t^*$ . We use default values of  $Pe_w = 1$ ,  $St_w = 1$ ,  $St_i = 1$ ,  $\mathcal{F} = 0.75$ . Inset (a) and (b) use  $St_w = 0.75$  while insets (c) and (d) use  $St_i = 0.9$ .



# Chapter 5

## Summary, conclusions and outlook

### 5.1 Summary and conclusions

The motivation of this TFR was to firstly examine some of the fundamental research literature on ice crystal icing, and the secondly, to examine and extend a recent numerical work by [Bucknell et al. \[2019a,c,b\]](#) where a simple one-dimensional three-layer model of ice crystal icing was proposed. Our first objective was to make the Bucknell *et al.* formulation more rigorous and systematic by beginning with the general framework of [Myers et al. \[2002\]](#) for thin-film flows on curved surfaces. In particular this would allow us, in the future, to consider more general two-dimensional interfaces on curved substrates such as aerofoils.

Next, this formulation was coupled with the three-layer ice-crystal model of Bucknell *et al.* except with a few differences: (i) we provide more justification for some of the assumptions discussed previously; (ii) we formally non-dimensionalise the problem and isolate key non-dimensional quantities such as the Peclet number, the Stefan number, and key scalings on lengths, times, and so forth. Finally, we developed a systematic approximation procedure to this problem using asymptotic analysis in the limit of small Peclet number.

Our last objective was to simulate numerically our designed model. The domain in question was both growing over time, in addition with the interface between layers moving over time. We re-scaled our PDE and wrote our temperature profile in terms of a single profile dependent on each sub-interval within the re-scaled domain. We then briefly examined the effect that key parameters such as the Stefan number, Peclet number and the heat source term have on the growth of the water and ice layers.

The work during this TFR has motivated a number of interesting and deep questions about the mathematical modelling of engine ice crystal formation. During the PhD we intend to pursue a number of the following directions:

1. Systematic parameter sweep and a complete set of asymptotics for the key parameters,
2. Mathematical models of ice crystals on more general geometries,
3. Numerics to incorporate sophisticated geometries and additional physics,
4. Mathematical models of ice breakoff,
5. Model development in parallel with experiments.

We provide additional discussion of some of the above components in the following section.

## 5.2 Future Work

We introduced the directions for future analysis in the previous section which can be broken down into two main categories. There is the natural progression of what should be studied next, in addition to the long term goals.

### 5.2.1 Next Steps

From the work done in this report, the first two objectives follow naturally. Regarding the first direction, we already obtained preliminary results on the effect of adjusting key parameters. This can be extended to a systematic exploration of the space of solutions. In addition, exploring different boundary conditions and how it affects the growth of the different layers and temperature profiles. Following this, exploring asymptotics for different key quantities. We have already studied small Peclet number, but examining this in conjunction with different Stefan regimes would be the next logical step. Finally we would perform a comprehensive comparison between both the asymptotics and the numerics.

For the second direction we shift to a two-dimensional system, where the initial step moving forward is to go back to the thin film governing equation given by Equation 3.1 and consider the two-dimensional case. Examining the system from a one-dimensional perspective loses much of the interesting features of the full system, for example, in that frame, there is no clear length-scale from which to choose from and we essentially ignore the incoming flow field.

As we extend our model to further dimensions this broadens the scope of what can be explored. We can incorporate different geometries present in an engine, whether they be weakly curved or cylindrical. For each of the geometries this presents the challenge of specifying the shape in the coordinate system and the subsequently solving the equations. As we consider an engine, this also presents different elements such as angle of incline, flow on top or bottom as well as leading or trailing edge. In the case of stators, exploring how the distance from the boundaries affects accretion especially with relation to the flow field.

### 5.2.2 Long Term

In the long term we want the model we develop to capture the essence of the different physical processes of ice crystal icing. These take on the aspects from challenges three to five which include (i) more sophisticated numerics; (ii) modelling the break off of ice and; (iii) development in parallel with experiments.

Currently for our one-dimensional simulation we use the finite difference method. If we try to incorporate more general complex geometries, more than likely our current system would be insufficient. It is probable that to effectively implement such geometries this would require using the finite element method. From examining the literature, most other groups studying ICI have implemented some form of particle tracking to simulate more realistic flow field. We would either seek to use the available resources or implement our own version.



Thus far, there is very little mentioned in the literature concerning the breaking off of ice. However, this is an element which is of special interest to flight industries, since it is this break off that is responsible for a lot of the damage dealt to engines. In the long term we would seek to model this behaviour and identify the key parameters that are responsible for the threshold of ice break off.

Ultimately, we wish to improve on the current state of the art knowledge in the field of ICI. Studying different accretion models for different geometries and developing numerics for complicated simulation provide very interesting challenges and results. However, we wish to validate any analytical or numerical results arising from our developed model with experimental results and the available experimental data.



# Bibliography

- E. Ayan and S. Özgen. In-flight ice accretion simulation in mixed-phase conditions. *The Aeronautical Journal*, 122(1249):409–441, 2018.
- A. Baumert, S. Bansmer, P. Trontin, and P. Villedieu. Experimental and numerical investigations on aircraft icing at mixed phase conditions. *International Journal of Heat and Mass Transfer*, 123:957–978, 2018.
- T.W. Brakel, J.P.F Charpin, and T. G. Myers. One-dimensional ice growth due to incoming supercooled droplets impacting on a thin conducting substrate. *International Journal of Heat and Mass Transfer*, 50(9-10):1694–1705, 2007.
- A. Bucknell, M. McGilvray, D. Gillespie, G. Jones, and B. Collier. A three-layer thermodynamic model for ice crystal accretion on warm surfaces: Emm-c. Technical report, SAE Technical Paper, 2019a.
- A. Bucknell, M. McGilvray, D. Gillespie, L. Parker, P. Forsyth, H. S. Ifti, G. Jones, B. Collier, and A. Reed. Experimental study and analysis of ice crystal accretion on a gas turbine compressor stator vane. Technical report, SAE Technical Paper, 2019b.
- A. Bucknell, M. McGilvray, D. Gillespie, X. Yang, G. Jones, and B. Collier. Icicle: A model for glaciated & mixed phase icing for application to aircraft engines. Technical report, SAE Technical Paper, 2019c.
- T. Currie, D. Knezevici, D. Fuleki, P. M. Struk, A. P. Broeren, J.-C. Tsao, M. Vargas, and W. Wright. Fundamental ice crystal accretion physics studies. In *SAE 2011 International Conference on Aircraft and Engine Icing and Ground Deicing*, 2011.
- T. C Currie, D. Fuleki, D. C. Knezevici, and J. D. MacLeod. Altitude scaling of ice crystal accretion. In *5th AIAA Atmospheric and Space Environments Conference*, page 2677, 2013.

- T. C. Currie, D. Fuleki, and A. Mahallati. Experimental studies of mixed-phase sticking efficiency for ice crystal accretion in jet engines. In *6th AIAA Atmospheric and Space Environments Conference*, page 3049, 2014.
- T.C. Currie and D. Fuleki. Development and application of an impedance-based instrument for measuring the liquid fraction and thickness of ice crystal accretions. Technical report, SAE Technical Paper, 2015.
- T.C. Currie, P. Struk, J.-C. Tsao, D. Fuleki, and D. Knezevici. Fundamental study of mixed-phase icing with application to ice crystal accretion in aircraft jet engines. In *4th AIAA Atmospheric and Space Environments Conference*, page 3035, 2012.
- R. W. Gent, N. P. Dart, and J. T. Cansdale. Aircraft icing. *Philosophical Transactions of the Royal Society of London. Series A: Mathematical, Physical and Engineering Sciences*, 358 (1776):2873–2911, 2000.
- A. Grandin and F. Dezitter. Airbus HAIC. [https://trimis.ec.europa.eu/sites/default/files/project/documents/20121116\\_120049\\_92680\\_HAIC.pdf](https://trimis.ec.europa.eu/sites/default/files/project/documents/20121116_120049_92680_HAIC.pdf), 2011. [Online; accessed 03-September-2021].
- D. M. Kintea, T. Hauk, I. V. Roisman, and C. Tropea. Shape evolution of a melting nonspherical particle. *Physical Review E*, 92(3):033012, 2015.
- D. Leroy, E. Fontaine, A. Schwarzenboeck, J. W. Strapp, L. Lilie, J. Delanoë, A. Protat, F. Dezitter, and A. Grandin. Haic/hiwc field campaign-specific findings on psd microphysics in high iwc regions from in situ measurements: Median mass diameters, particle size distribution characteristics and ice crystal shapes. In *SAE 2015 International Conference on Icing of Aircraft, Engines, and Structures*, pages SAE–Technical, 2015.
- J. G. Mason, P. Chow, and D. M Fuleki. Understanding ice crystal accretion and shedding phenomenon in jet engines using a rig test. *Journal of Engineering for Gas Turbines and Power*, 133(4), 2011.
- J.G. Mason, W. Strapp, and P. Chow. The ice particle threat to engines in flight. In *44th AIAA Aerospace Sciences Meeting and Exhibit*, page 206, 2006.
- R. Mazzawy. Modeling of ice accretion and shedding in turbofan engines with mixed phase/glaciated (ice crystal) conditions. *SAE Technical Paper*, (2007-01):3288, 2007.

- B.L. Messinger. Ice prevention as related to airframe design-1952. Technical report, SAE Technical Paper, 1952.
- B.L. Messinger. Equilibrium temperature of an unheated icing surface as a function of air speed. *Journal of the Aeronautical Sciences*, 20(1):29–42, 1953.
- T.G Myers, J.P.F. Charpin, and S.J. Chapman. The flow and solidification of a thin fluid film on an arbitrary three-dimensional surface. *Physics of Fluids*, 14(8):2788–2803, 2002.
- NRCC. RATFac. <https://nrc.canada.ca/en/research-development/nrc-facilities/research-altitude-test-facility>, 2019. [Online; accessed 03-September-2021].
- M. J. Oliver. *A Study on the Physics of Ice Accretion in a Turbofan Engine Environment*. Case Western Reserve University, 2013.
- M. Tribus. *Intermittent heating for protection in aircraft icing*. PhD thesis, University of California, Los Angeles–Engineering, 1949.
- P. Trontin and P. Villedieu. A comprehensive accretion model for glaciated icing conditions. *International Journal of Multiphase Flow*, 108:105–123, 2018.
- C. Vuik. Some historical notes about the stefan problem. 1993.
- W. Wright, M. Potapczuk, and L. Levinson. Comparison of lewice and glennice in the sld regime. In *46th AIAA Aerospace Sciences Meeting and Exhibit*, page 439, 2008.
- W. Wright, P. Jorgenson, and J. Veres. Mixed phase modeling in glennice with application to engine icing. In *AIAA Atmospheric and Space Environments Conference*, page 7674, 2010.



# Appendix A

Examining an arbitrary surface we parameterise using a curvilinear coordinate system. Given a substrate  $\mathcal{S}$ , we examine the lines of principal curvature and parameterise these using the variables  $s_1, s_2$ , where there is a mapping from these coordinates to the standard cartesian coordinates

$$\begin{aligned}s_1 &= s_1(x, y, z), \\ s_2 &= s_2(x, y, z).\end{aligned}$$

**Note:** For a surface, the directions in which the curvature takes its maximum and minimum values in the normal plane, are call the principal directions. These are always orthogonal to each other.

We then can denote the position of any point on the substrate as  $\mathbf{R} = \mathbf{R}(s_1, s_2)$ . Our first two unit orthogonal vectors  $\mathbf{e}_1$  and  $\mathbf{e}_2$  we define to be tangential to  $s_1$  and  $s_2$ . We define our third to be the normal to  $\mathcal{S}$  and thus we can write a point in space as

$$\mathbf{r}(s_1, s_2, s_3) = \mathbf{R}(s_1, s_2) + \eta \mathbf{n},$$

where  $\eta$  gives the distance away from substrate along the normal to the substrate. We recover our substrate when  $\eta = 0$ .

Following Myers [Myers et al. \[2002\]](#) we use the fundamental forms of the surface,

$$\begin{aligned}E &= \mathbf{R}_1 \cdot \mathbf{R}_1, & F &= \mathbf{R}_1 \cdot \mathbf{R}_2, & G &= \mathbf{R}_2 \cdot \mathbf{R}_2, \\ L &= \mathbf{R}_{11} \cdot \mathbf{n}, & M &= \mathbf{R}_{12} \cdot \mathbf{n}, & N &= \mathbf{R}_{22} \cdot \mathbf{n}\end{aligned},$$

where we define

$$\mathbf{R}_1 \equiv \frac{\partial \mathbf{R}}{\partial s_1}, \quad \mathbf{R}_2 \equiv \frac{\partial \mathbf{R}}{\partial s_2}$$

and

$$\mathbf{n} = \frac{\mathbf{R}_1 \wedge \mathbf{R}_2}{|\mathbf{R}_1 \wedge \mathbf{R}_2|} = \frac{\mathbf{R}_1 \wedge \mathbf{R}_2}{(EG - F^2)^{1/2}}$$

is the outward pointing normal. The curvature is then defined by the relation

$$\kappa_1 = \frac{L}{E}, \quad \kappa_2 = \frac{N}{G}.$$